01 Jan 2007

The Dynamics and Interaction of Quantized Vortices in the Ginzburg-Landau-Schrödinger Equation

Yanzhi Zhang
Missouri University of Science and Technology, zhangyanz@mst.edu

Weizhu Bao

Qiang Du

Recommended Citation

Y. Zhang et al., "The Dynamics and Interaction of Quantized Vortices in the Ginzburg-Landau-Schrödinger Equation," *SIAM Journal on Applied Mathematics*, Society for Industrial and Applied Mathematics (SIAM), Jan 2007.
The definitive version is available at https://doi.org/10.1137/060671528

SIAM J. APPL. MATH.
Vol. 67, No. 6, pp. 1740–1775

THE DYNAMICS AND INTERACTION OF QUANTIZED VORTICES IN THE GINZBURG–LANDAU–SCHRÖDINGER EQUATION*

YANZHI ZHANG†, WEIZHU BAO‡, AND QIANG DU§

Abstract. The dynamic laws of quantized vortex interactions in the Ginzburg–Landau–Schrödinger equation (GLSE) are analytically and numerically studied. A review of the reduced dynamic laws governing the motion of vortex centers in the GLSE is provided. The reduced dynamic laws are solved analytically for some special initial data. By directly simulating the GLSE with an efficient and accurate numerical method proposed recently in [Y. Zhang, W. Bao, and Q. Du, *Numerical simulation of vortex dynamics in Ginzburg–Landau–Schrödinger equation*, European J. Appl. Math., to appear], we can qualitatively and quantitatively compare quantized vortex interaction patterns of the GLSE with those from the reduced dynamic laws. Some conclusive findings are obtained, and discussions on numerical and theoretical results are made to provide further understanding of vortex interactions in the GLSE. Finally, the vortex motion under an inhomogeneous potential in the GLSE is also studied.

Key words. Ginzburg–Landau equation, nonlinear Schrödinger equation, complex Ginzburg–Landau equation, Ginzburg–Landau–Schrödinger equation, vortex state, reduced dynamic laws, vortex interaction

AMS subject classifications. 35Q55, 65T99, 65Z05, 65N12, 65N35, 81-08

DOI. 10.1137/060671528

1. Introduction.

One of the most well-studied equations in nonlinear science is the Ginzburg–Landau–Schrödinger equation (GLSE) of the form [36]

$$(\alpha - i\beta)\partial_t \psi(\mathbf{x}, t) = \nabla^2 \psi + \frac{1}{\varepsilon^2}\left(V(\mathbf{x}) - |\psi|^2\right)\psi, \qquad \mathbf{x} \in \mathbb{R}^2, \quad t > 0, \tag{1.1}$$

$$\psi(\mathbf{x}, 0) = \psi_0(\mathbf{x}), \qquad \mathbf{x} \in \mathbb{R}^2. \tag{1.2}$$

Here, t is time, $\mathbf{x} = (x, y)^T \in \mathbb{R}^2$ is the Cartesian coordinate vector, (r, θ) is the polar coordinate system, $\psi = \psi(\mathbf{x}, t)$ is a complex-valued wave function (or order parameter), $V(\mathbf{x})$ is a real-valued external potential satisfying $\lim_{|\mathbf{x}|\to\infty} V(\mathbf{x}) = 1$, $\varepsilon > 0$ is a constant, and α and β are two nonnegative constants satisfying $\alpha + \beta > 0$. A vortex-like solution satisfies a nonzero far-field condition as follows: For a given integer $m \in \mathbb{Z}$,

$$|\psi(\mathbf{x}, t)| \to 1 \text{ (e.g., } \psi \to e^{im\theta}), \quad t \geq 0, \quad \text{when } r = |\mathbf{x}| = \sqrt{x^2 + y^2} \to \infty. \tag{1.3}$$

The GLSE (1.1) describes a large variety of nonlinear phenomena, including nonlinear waves, phase transitions, superconductivity, superfluidity, liquid crystals, and

*Received by the editors October 5, 2006; accepted for publication (in revised form) May 22, 2007; published electronically October 5, 2007. We acknowledge support from National University of Singapore grant R-146-000-083-112, and from NSF-DMS 0409297, NSF-CCF 0430349, and NSF-DMR 0205232.

http://www.siam.org/journals/siap/67-6/67152.html

†Department of Mathematics, National University of Singapore, Singapore 117543 (zhyanzhi@gmail.com).

‡Department of Mathematics and Center for Computational Science and Engineering, National University of Singapore, Singapore 117543 (bao@math.nus.edu.sg, http://www.math.nus.edu.sg/~bao).

§Department of Mathematics, Pennsylvania State University, University Park, PA 16802 (qdu@math.psu.edu, http://www.math.psu.edu/qdu).

strings in the field theory. For example, when $\alpha = 1$ and $\beta = 0$, it collapses into the nonlinear heat equation (NLHE) or the Ginzburg–Landau equation (GLE) [27, 28]. The GLE with a complex order parameter is well known for modeling superconductivity [10, 11, 14, 12, 19], while that with a real order parameter corresponds to the Allen–Cahn equation in phase transition [13]. When $\alpha = 0$ and $\beta = 1$, the GLSE reduces to the nonlinear Schrödinger equation (NLSE) [27, 31, 22] for modeling, for example, superfluidity or Bose–Eistein condensation (BEC). While $\alpha > 0$ and $\beta > 0$, it is the complex Ginzburg–Landau equation (CGLE), or NLSE with a damping term [3], which also arises in the study of the hydrodynamic instability [1].

It is known that there are stationary *vortex solutions* with a single winding number or index $m \in \mathbb{Z}$ of the GLSE (1.1) with $\varepsilon = 1$ and $V(\mathbf{x}) \equiv 1$ [27, 14, 36], which take the form

$$\phi_m(\mathbf{x}) = f_m(r)\, e^{im\theta}, \qquad \mathbf{x} = (r\cos\theta, r\sin\theta)^T \in \mathbb{R}^2, \tag{1.4}$$

where the modulus $f_m(r)$ is a real-valued function satisfying

$$\frac{1}{r}\frac{d}{dr}\left(r\frac{df_m(r)}{dr}\right) - \frac{m^2}{r^2} f_m(r) + \left(1 - f_m^2(r)\right) f_m(r) = 0, \qquad 0 < r < \infty, \tag{1.5}$$

$$f_m(0) = 0, \qquad f_m(r) = 1 \quad \text{when} \quad r \to \infty. \tag{1.6}$$

The modulus as well as the core sizes of such vortex states have been calculated in the literature [27, 36] by numerically solving the boundary value problem (1.5)–(1.6). Numerical and analytical results suggest that the vortex states with winding number $m = \pm 1$ are dynamically stable, and, respectively, $|m| > 1$ dynamically unstable [27, 34, 25, 26, 22, 2, 36] (note that the stability and interaction laws of a quantized vortex in the Gross–Pitaevskii equation for BEC [3, 4, 5] may be very different from that studied here due to the different far-field boundary conditions).

In this paper, we study the GLSE (1.1) with initial conditions containing several, say N, vortices. A precise definition of vortex solutions can be found in [22, 19]. We are mainly concerned with the following initial condition:

$$\psi_0(\mathbf{x}) = \prod_{j=1}^{N} \phi_{m_j}\left(\mathbf{x} - \mathbf{x}_j^0\right) = \prod_{j=1}^{N} \phi_{m_j}\left(x - x_j^0,\, y - y_j^0\right), \qquad \mathbf{x} \in \mathbb{R}^2, \tag{1.7}$$

where N is the total number of vortices and ϕ_{m_j} is the vortex state as defined in (1.4) with winding number $m_j = \pm 1$ (see [36] for their numerical solutions). We may then consider the interaction of N vortices with their initial centers shifted from the origin $(0,0)$ to $\mathbf{x}_j^0 = \left(x_j^0, y_j^0\right)^T$ $(1 \le j \le N)$. Taking $m = \sum_{j=1}^{N} m_j$ in (1.3), we refer to vortices with the same winding numbers as *like vortices* and those with different winding numbers as *opposite vortices*.

When $\varepsilon = 1$ and $V(\mathbf{x}) \equiv 1$ in (1.1), it is known that for N well-separated vortices of winding numbers $m_j = \pm 1$ and locations $\mathbf{x}_j$ $(1 \le j \le N)$, the leading asymptotic expansion of the energy is

$$E \sim \sum_{j=1}^{N} E_j - \pi \sum_{j \ne l} m_j\, m_l \ln\left|\mathbf{x}_l - \mathbf{x}_j\right|, \tag{1.8}$$

where E_j is the self-energy of the vortex at $\mathbf{x}_j$, and the second term corresponds to the well-known Kirchoff–Onsager Hamiltonian. From (1.8), we can obtain the

vortex dynamic laws of the induced motion in the leading order, i.e., the adiabatic approximation [27]. For the GLE, i.e., $\alpha = 1$ and $\beta = 0$ in (1.1), the vortex dynamics satisfies [27, 14, 15, 19]

$$\kappa \mathbf{v}_j(t) := \kappa \frac{d\mathbf{x}_j(t)}{dt} = 2m_j \sum_{l=1,\, l\neq j}^{N} m_l \frac{\mathbf{x}_j(t) - \mathbf{x}_l(t)}{|\mathbf{x}_j(t) - \mathbf{x}_l(t)|^2}, \qquad t \geq 0, \tag{1.9}$$

$$\mathbf{x}_j(0) = \mathbf{x}_j^0, \qquad 1 \leq j \leq N, \tag{1.10}$$

where κ is a constant determined from the initial setup (1.7). On the other hand, for the NLSE, i.e., $\alpha = 0$ and $\beta = 1$ in (1.1), it satisfies [27, 14, 8, 19]

$$\mathbf{v}_j(t) := \frac{d\mathbf{x}_j(t)}{dt} = 2 \sum_{l=1,\, l\neq j}^{N} m_l \frac{\mathbf{J}\,(\mathbf{x}_j(t) - \mathbf{x}_l(t))}{|\mathbf{x}_j(t) - \mathbf{x}_l(t)|^2}, \qquad t \geq 0, \tag{1.11}$$

$$\mathbf{x}_j(0) = \mathbf{x}_j^0, \qquad 1 \leq j \leq N, \tag{1.12}$$

where $\mathbf{J}$ is a symplectic matrix defined as

$$\mathbf{J} = \begin{pmatrix} 0 & -1 \\ 1 & 0 \end{pmatrix}. \tag{1.13}$$

For asymptotic study of the vortex motions in the GLE and the NLSE, we refer to [7, 8, 9, 6, 20, 18, 29, 31, 32, 33, 35] and references therein.

The aim of this paper is to provide a more detailed and accurate account of the vortex dynamics governed by the GLSE, in particular, to address some open questions concerning the range of validity of the reduced dynamic laws. Our approach is to first solve analytically the ordinary differential equations (ODEs) (1.9) and (1.11) for any N under a few types of initial data, and then compare these solutions with those from direct simulation results of the GLSE (1.1) by using the efficient and accurate numerical method proposed recently in [36]. The key features of the numerical method include (i) the application of a time-splitting technique for decoupling the nonlinearity in the GLSE; (ii) the adoption of polar coordinates to effectively match and resolve the nonzero far-field conditions (1.3) in phase space; and (iii) the utilization of Fourier pseudospectral discretization in the transverse direction and a second order (or fourth order) finite difference or (finite element) discretization in the radial direction [36].

There are naturally many interesting issues concerning the vortex dynamics in various limiting cases, such as the interaction of well-separated vortices with smaller and smaller vortex cores ($\varepsilon \to 0$), and when the distances between the vortices become comparable with the core sizes (initially, both ε and the distances are of $O(1)$). Our approach and numerical methods are applicable to both of these situations, but due to page limitation, our main focus here is on the latter and we leave the discussion on the former to future studies. The main findings in this paper provide justification of the asymptotic vortex dynamic laws in some situations while unveiling limitations in other cases; they also reveal interesting phenomena on the sound wave propagation and the radiation effect associated with the vortex interaction.

The results of the paper are organized as follows. In section 2, based on the nonlinear ODEs of the reduced dynamic laws, we prove the conservation of the mass center and signed mass center of the N vortex centers, respectively, and solve analytically the reduced dynamic laws with a few types of initial data. In section 3, the dynamics and interaction of quantized vortices in the GLE are directly simulated by

solving (1.1) and compared with those from the reduced dynamic laws. Similar results for the NLSE are reported in section 4. The vortex motions in the CGLE, and in the GLSE under an inhomogeneous external potential, are reported in section 5. Finally, some conclusions are drawn in section 6.

2. The reduced dynamic laws. In this section, we first prove the conservation of the mass center and signed mass center of the N vortex centers in the reduced dynamic laws (1.9) and (1.11) for the GLE and the NLSE, respectively. These conservation properties can be used to solve the dynamic laws in special cases and to compare with the direct numerical simulation results of the GLE and the NLSE. We then solve the nonlinear ODEs analytically for several special types of initial data; such analytical solutions can again be compared with the numerical solutions of the GLE and the NLSE.

2.1. Conservation laws. Define, respectively, the mass center $\overline{\mathbf{x}}$ and the signed mass center $\widetilde{\mathbf{x}}$ of the N vortices as

$$\overline{\mathbf{x}}(t) := \frac{1}{N}\sum_{j=1}^{N}\mathbf{x}_j(t) \quad \text{and} \quad \widetilde{\mathbf{x}}(t) := \frac{1}{N}\sum_{j=1}^{N} m_j\,\mathbf{x}_j(t). \tag{2.1}$$

Let

$$Z_j = \sum_{l=1,\, l\neq j}^{N} m_l \frac{\mathbf{x}_j(t)-\mathbf{x}_l(t)}{|\mathbf{x}_j(t)-\mathbf{x}_l(t)|^2}.$$

It is easy to see that

$$\sum_{j=1}^{N} m_j Z_j = \sum_{j=1}^{N-1}\sum_{j<1\le N}^{N} m_j\, m_l \left[\frac{\mathbf{x}_j(t)-\mathbf{x}_l(t)}{|\mathbf{x}_j(t)-\mathbf{x}_l(t)|^2} + \frac{\mathbf{x}_l(t)-\mathbf{x}_j(t)}{|\mathbf{x}_l(t)-\mathbf{x}_j(t)|^2}\right] = 0. \tag{2.2}$$

Then we have the following.

LEMMA 2.1. *The mass center of the N vortices in the reduced dynamic laws* (1.9) *for the GLE is conserved, i.e.,*

$$\overline{\mathbf{x}}(t) := \frac{1}{N}\sum_{j=1}^{N}\mathbf{x}_j(t) \equiv \overline{\mathbf{x}}(0) := \frac{1}{N}\sum_{j=1}^{N}\mathbf{x}_j(0) = \frac{1}{N}\sum_{j=1}^{N}\mathbf{x}_j^0, \qquad t \ge 0. \tag{2.3}$$

Proof. Summing (1.9) for $1 \le j \le N$ and noting (2.1) and (2.2), we get for $t \ge 0$,

$$\frac{d\overline{\mathbf{x}}(t)}{dt} = \frac{1}{N}\sum_{j=1}^{N}\frac{d\mathbf{x}_j(t)}{dt} = \frac{2}{\kappa N}\sum_{j=1}^{N} m_j Z_j = 0.$$

Thus the conservation law (2.3) is a combination of the above and (1.7). ∎

Similarly, we have the following.

LEMMA 2.2. *The signed mass center of the N vortices in the reduced dynamic laws* (1.11) *for the NLSE is conserved, i.e.,*

$$\widetilde{\mathbf{x}}(t) := \frac{1}{N}\sum_{j=1}^{N} m_j\,\mathbf{x}_j(t) \equiv \widetilde{\mathbf{x}}(0) := \frac{1}{N}\sum_{j=1}^{N} m_j\,\mathbf{x}_j(0) = \frac{1}{N}\sum_{j=1}^{N} m_j\,\mathbf{x}_j^0, \quad t \ge 0. \tag{2.4}$$

Proof. Multiplying (1.11) by $m_j N \mathbf{J}^{-1}$, summing (1.11) for $1 \le j \le N$, and noting (2.1) and (2.2), we have for $t \ge 0$,

$$N\mathbf{J}^{-1}\frac{d\widetilde{\mathbf{x}}(t)}{dt} = \sum_{j=1}^{N} m_j \mathbf{J}^{-1}\frac{d\mathbf{x}_j(t)}{dt} = 2\sum_{j=1}^{N} m_j Z_j = 0.$$

Thus the conservation law (2.4) is a combination of the above and (1.7). ∎

2.2. Initial conditions used for the study of vortex dynamics. Due to the special structures of the nonlinear ODEs (1.9) and (1.11), we can solve them analytically when the N vortices are initially located symmetrically on a circle or at its center. By the conservation of the mass center and signed mass center in (1.9) and (1.11), we assume without loss of generality that the circle is centered at the origin with radius $r_0 = a > 0$.

For simplicity, we denote θ_0 as a given constant, denote $m_0 = +1$ or -1, and consider the following five patterns for the initial conditions in (1.7).

Pattern I. N ($N \ge 2$) like vortices uniformly located on a circle, i.e.,

$$\mathbf{x}_j^0 = a\left(\cos\left(\frac{2j\pi}{N}+\theta_0\right), \sin\left(\frac{2j\pi}{N}+\theta_0\right)\right)^T, \quad \text{and } m_j = m_0 \quad \text{for } 1 \le j \le N. \tag{2.5}$$

Pattern II. N ($N \ge 3$) like vortices located on a circle and its center, i.e.,

$$\mathbf{x}_N^0 = (0,0)^T, \qquad m_{_N} = m_0, \tag{2.6}$$

and for $1 \le j \le N-1$,

$$\mathbf{x}_j^0 = a\left(\cos\left(\frac{2j\pi}{N-1}+\theta_0\right), \sin\left(\frac{2j\pi}{N-1}+\theta_0\right)\right)^T \quad \text{with} \quad m_j = m_0. \tag{2.7}$$

Pattern III. The same as Pattern II, except $m_{_N} = -m_0$ for the center vortex.

Pattern IV. Two opposite vortices, i.e., for $j = 1, 2$,

$$\mathbf{x}_j^0 = a\left(\cos\left(j\pi+\theta_0\right), \sin\left(j\pi+\theta_0\right)\right)^T \quad \text{with} \quad m_1 = -m_2 = m_0. \tag{2.8}$$

Pattern V. Three vortices ($N = 3$) with nonsymmetric initial setups.

Here we consider the following three different cases (with $m_1 = m_3 = +1$):

Case 1. $\mathbf{x}_1^0 = (-a, -b/2)^T$, $\mathbf{x}_2^0 = (0, b)^T$, $\mathbf{x}_3^0 = (a, -b/2)^T$, $m_2 = +1$.

Case 2. $\mathbf{x}_1^0 = (-\sqrt{3}a/2, -a/2)^T$, $\mathbf{x}_2^0 = (0, a)^T$, $\mathbf{x}_3^0 = (\sqrt{3}a/2, -a/2)^T$, $m_2 = -1$.

Case 3. $\mathbf{x}_1^0 = (-a, -b/2)^T$, $\mathbf{x}_2^0 = (0, b)^T$, $\mathbf{x}_3^0 = (a, -b/2)^T$, $m_2 = -1$.

Notice that for all five types of patterns, we have $\overline{\mathbf{x}}(t) = \overline{\mathbf{x}}(0) = (0,0)^T$ for $t \ge 0$. Moreover, for the first three patterns and the first case of Pattern V, we have $\widetilde{\mathbf{x}}(t) = \widetilde{\mathbf{x}}(0) = 0$.

2.3. Analytical solutions of the reduced dynamics for the GLE. Noting (2.3), we can solve the nonlinear ODEs (1.9) analytically when the initial conditions in (1.10) are given by Patterns I–IV.

LEMMA 2.3. *If the initial data in* (1.10) *satisfy* (2.5)*, i.e., Pattern* I*, then the solutions of* (1.9)–(1.10) *can be given, for* $1 \le j \le N$ *with* $N \ge 2$*, by*

$$\mathbf{x}_j(t) = \sqrt{a^2 + \frac{2\,(N-1)}{\kappa}\,t}\,\left(\cos\left(\frac{2j\pi}{N}+\theta_0\right), \sin\left(\frac{2j\pi}{N}+\theta_0\right)\right)^T, \quad t \ge 0. \tag{2.9}$$

Proof. For any $N \geq 2$, based on the structures of the ODEs (1.9) and the initial data (2.5), we take the ansatz for the solution as

$$\mathbf{x}_j(t) = c_{_N}(t)\mathbf{x}_j^0, \qquad t \geq 0, \quad 1 \leq j \leq N, \tag{2.10}$$

where $c_{_N}(t)$ is a function of time t and $c_{_N}(0) = 1$. Substituting (2.10) into (1.9), applying a dot-product on both sides by $\mathbf{x}_j^0$, and noting (2.5), we get

$$\begin{aligned} c_{_N}'(t) &= \frac{2}{\kappa a^2 c_{_N}(t)} \sum_{l=1,\, l\neq j}^{N} m_j m_l \frac{(\mathbf{x}_j^0 - \mathbf{x}_l^0)\cdot \mathbf{x}_j^0}{|\mathbf{x}_j^0 - \mathbf{x}_l^0|^2} \\ &= \frac{2}{\kappa a^2 c_{_N}(t)} \sum_{l=1,\, l\neq j}^{N} \frac{a^2 - \mathbf{x}_l^0 \cdot \mathbf{x}_j^0}{2a^2 - 2\mathbf{x}_l^0 \cdot \mathbf{x}_j^0} = \frac{N-1}{\kappa a^2 c_{_N}(t)}, \quad t \geq 0. \end{aligned}$$

Solving the above ODE and noting that $c_{_N}(0) = 1$, we obtain

$$c_{_N}(t) = \sqrt{1 + \frac{2(N-1)}{a^2\kappa}\, t}, \qquad t \geq 0. \tag{2.11}$$

Thus the solution (2.9) is a combination of (2.10), (2.11), and (2.5). ∎

From the results in Lemma 2.3 we can see that, when the N vortices are uniformly located on a circle initially, i.e., as in Pattern I, by the reduced dynamic law each vortex moves outside along the line passing through its initial location and the origin, and these N vortices are located on a circle at any time t with its radius increasing by time $c_{_N}(t)$ as in (2.11).

LEMMA 2.4. *If the initial data in* (1.10) *satisfy* (2.6)–(2.7)*, i.e., Pattern* II*, then the solutions of* (1.9)–(1.10) *are*

$$\mathbf{x}_N(t) \equiv (0,0)^T, \qquad t \geq 0, \tag{2.12}$$

and for $1 \leq j \leq N-1$ *with* $N \geq 3$*,*

$$\mathbf{x}_j(t) = \sqrt{a^2 + \frac{2N}{\kappa}\, t}\, \left(\cos\left(\frac{2j\pi}{N-1} + \theta_0\right), \sin\left(\frac{2j\pi}{N-1} + \theta_0\right)\right)^T, \quad t \geq 0. \tag{2.13}$$

Proof. Due to the symmetry of the ODEs (1.9), the initial data (2.5), and the conservation of mass center (2.3), we can immediately obtain the solution (2.12). As in the proof of Lemma 2.3, we assume

$$\mathbf{x}_j(t) = d_N(t)\mathbf{x}_j^0, \qquad t \geq 0, \quad 1 \leq j \leq N-1,$$

where $d_N(t)$ is a function of time t and $d_N(0) = 1$. Substituting the above into (1.9), applying a dot-product on both sides by $\mathbf{x}_j^0$, and noting (2.7) and (2.12), we get

$$\begin{aligned} d_N'(t) &= \frac{2}{\kappa a^2 d_N(t)} \left[m_j m_{_N} \frac{(\mathbf{x}_j^0 - \mathbf{x}_N^0)\cdot \mathbf{x}_j^0}{|\mathbf{x}_j^0 - \mathbf{x}_N^0|^2} + \sum_{l=1,\, l\neq j}^{N-1} m_j m_l \frac{(\mathbf{x}_j^0 - \mathbf{x}_l^0)\cdot \mathbf{x}_j^0}{|\mathbf{x}_j^0 - \mathbf{x}_l^0|^2} \right] \\ &= \frac{2}{\kappa a^2 d_N(t)} \left[m_0^2 + \sum_{l=1,\, l\neq j}^{N-1} m_0^2 \frac{a^2 - \mathbf{x}_l^0 \cdot \mathbf{x}_j^0}{2a^2 - 2\mathbf{x}_l^0 \cdot \mathbf{x}_j^0} \right] = \frac{N}{\kappa a^2 d_N(t)}, \quad t \geq 0. \end{aligned}$$

Solving the above ODE and noting that $d_N(0) = 1$, we obtain

$$d_N(t) = \sqrt{1 + \frac{2N}{a^2\kappa}\, t}, \qquad t \geq 0. \tag{2.14}$$

Thus the solution (2.13) is a combination of the above and (2.7). ∎

From the results in Lemma 2.4 we can see that, for the dynamics of (1.9)–(1.10) in Pattern II, by the reduced dynamic law the vortex initially at the center of the circle does not move for any time $t \geq 0$, each of the other $N-1$ vortices moves outside along the line passing through its initial location and the origin, and these $N-1$ vortices are located on a circle at any time t with its radius increasing by time $d_N(t)$ as in (2.14).

LEMMA 2.5. *If the initial data in* (1.10) *are as in Pattern* III*, then the solutions of* (1.9)–(1.10) *are*

$$\mathbf{x}_N(t) \equiv (0,0)^T, \qquad t \geq 0, \tag{2.15}$$

and for $1 \leq j \leq N-1$ *with* $N \geq 3$*,*

$$\mathbf{x}_j(t) = \sqrt{a^2 + \frac{2(N-4)}{\kappa}\, t}\, \left(\cos\left(\frac{2j\pi}{N-1} + \theta_0\right), \sin\left(\frac{2j\pi}{N-1} + \theta_0\right)\right)^T. \tag{2.16}$$

The proof follows from the analogous results in Lemma 2.4. From the results in Lemma 2.5 we can see that, for the dynamics of (1.9)–(1.10) in Pattern III, by the reduced dynamic law (i) the vortex initially at the origin does not move during the interaction, each of the other $N-1$ vortices moves along the line passing through its initial location and the origin, and these $N-1$ vortices are located on a circle at any time t; (ii) when $N = 3$, the two vortices with the same index move towards each other and collide with the vortex having the opposite index at the origin and at time $t = t_c = \kappa a^2/2$; (iii) when $N = 4$, all four vortices do not move but remain at their initial locations for any $t \geq 0$; and (iv) when $N \geq 5$, the $N-1$ vortices with the same index move outside and never collide with the vortex with the opposite index no matter how small the initial radius of the circle is.

LEMMA 2.6. *If the initial data in* (1.10) *satisfy* (2.8)*, i.e., Pattern* IV*, then the solutions of* (1.9)–(1.10) *can be given by*

$$\mathbf{x}_j(t) = \sqrt{a^2 - \frac{2}{\kappa}\, t}\, \left(\cos\left(j\pi + \theta_0\right), \sin\left(j\pi + \theta_0\right)\right)^T, \quad 0 \leq t \leq t_c, \quad j = 1, 2, \tag{2.17}$$

with $t_c = \kappa a^2/2$.

The proof is similar to that of Lemma 2.3. From the results in Lemma 2.6 we can see that, for the dynamics of (1.9)–(1.10) in Pattern IV, when $0 \leq t < t_c = a^2\kappa/2$ the two vortices move towards each other along a line passing through their initial locations and collide at the origin at time $t = t_c = O(a^2)$ according to the reduced dynamic law.

2.4. Analytical solutions of the reduced dynamics for the NLSE. Similarly, noting (2.4) we can also solve the nonlinear ODEs (1.11) analytically when the initial conditions in (1.12) are given by Patterns I–IV.

LEMMA 2.7. *If the initial data in* (1.12) *satisfy* (2.5)*, i.e., Pattern* I*, then the solutions of* (1.11)–(1.12) *can be given, for* $1 \leq j \leq N$ *with* $N \geq 2$*, by*

$$\mathbf{x}_j(t) = a\left(\cos\left(\frac{2j\pi}{N} + \theta_0 + \frac{m_0(N-1)}{a^2}\, t\right), \sin\left(\frac{2j\pi}{N} + \theta_0 + \frac{m_0(N-1)}{a^2}\, t\right)\right)^T. \tag{2.18}$$

Proof. For any $N \geq 2$, based on the structures of the ODEs (1.11) and the initial data (2.5), we take the ansatz for the solution with $1 \leq j \leq N$ as

$$\mathbf{x}_j(t) = a\left(\cos\left(\frac{2j\pi}{N} + \theta_0 + \alpha_N(t)\right), \sin\left(\frac{2j\pi}{N} + \theta_0 + \alpha_N(t)\right)\right)^T, \quad t \geq 0, \tag{2.19}$$

where $\alpha_N(t)$ is a function of time and $\alpha_N(0) = 0$.

Now, let $\mathbf{x}_j^{\perp}(t) = a\left(-\sin\left(\frac{2j\pi}{N} + \theta_0 + \alpha_N(t)\right), \cos\left(\frac{2j\pi}{N} + \theta_0 + \alpha_N(t)\right)\right)^T$. By (1.13), we have the elementary identity

$$\begin{aligned} &\sum_{l=1,\, l\neq j}^{N} m_0 \frac{\mathbf{x}_j^{\perp} \cdot (\mathbf{J}\mathbf{x}_j) - \mathbf{x}_j^{\perp} \cdot (\mathbf{J}\mathbf{x}_l)}{|\mathbf{x}_j|^2 + |\mathbf{x}_l|^2 - 2\mathbf{x}_j \cdot \mathbf{x}_l} \\ &= \sum_{l=1,\, l\neq j}^{N} m_0 \frac{1 - \cos\left(\frac{2(j-l)\pi}{N}\right)}{2 - 2\cos\left(\frac{2(j-l)\pi}{N}\right)} = \frac{m_0(N-1)}{2}. \end{aligned} \tag{2.20}$$

Inserting (2.19) into (1.11) and applying a dot-product on both sides with $\mathbf{x}_j^{\perp}(t)$, we get

$$\alpha_N'(t) = \frac{2}{a^2} \sum_{l=1,\, l\neq j}^{N} m_l \frac{\mathbf{x}_j^{\perp} \cdot [\mathbf{J}(\mathbf{x}_j - \mathbf{x}_l)]}{|\mathbf{x}_j - \mathbf{x}_l|^2} = \frac{m_0(N-1)}{a^2}, \qquad t \geq 0.$$

Solving the above ODE and noting that $\alpha_N(0) = 0$, we obtain $\alpha_N(t) = m_0(N-1)t/a^2$ for $t \geq 0$. Thus a combination of the above leads to the solution (2.18). ∎

From the results in Lemma 2.7 we can see that, when the N like vortices are uniformly located on a circle initially, i.e., for the dynamics of (1.11)–(1.12) in Pattern I, they rotate along the circle (counterclockwise if $m_0 = +1$ and clockwise if $m_0 = -1$) with angular frequency $\omega = (N-1)/a^2$ (cf. Figure 13(a),(d)).

LEMMA 2.8. *If the initial data in* (1.12) *satisfy* (2.6)–(2.7)*, i.e., Pattern* II*, then the solutions of* (1.11)–(1.12) *are*

$$\mathbf{x}_N(t) \equiv (0,0)^T, \qquad t \geq 0, \tag{2.21}$$

and for $1 \leq j \leq N-1$ *with* $N \geq 3$*,*

$$\mathbf{x}_j(t) = a\left(\cos\left(\frac{2j\pi}{N-1} + \theta_0 + \frac{m_0 N}{a^2}\, t\right), \sin\left(\frac{2j\pi}{N-1} + \theta_0 + \frac{m_0 N}{a^2}\, t\right)\right)^T. \tag{2.22}$$

Proof. Due to the symmetry of the ODEs (1.11), the initial data (2.6)–(2.7), and the conservation of signed mass center (2.4), we can immediately get the solution (2.21). As in the proof of Lemma 2.7, we assume for $1 \leq j \leq N-1$ that

$$\mathbf{x}_j(t) = a\left(\cos\left(\frac{2j\pi}{N-1} + \theta_0 + \beta_N(t)\right), \sin\left(\frac{2j\pi}{N-1} + \theta_0 + \beta_N(t)\right)\right)^T, \tag{2.23}$$

where $\beta_N(t)$ is a function of time and $\beta_N(0) = 0$. Inserting (2.23) into (1.11), applying a dot-product on both sides with

$$\mathbf{x}_j^{\perp}(t) = a\left(-\sin\left(\frac{2j\pi}{N-1} + \theta_0 + \beta_N(t)\right), \cos\left(\frac{2j\pi}{N-1} + \theta_0 + \beta_N(t)\right)\right)^T,$$

and noting (1.13), (2.21), and (2.20) (with N replaced by $N-1$), we get

$$\beta_N'(t) = \frac{2}{a^2}\left[m_{_N}\frac{\mathbf{x}_j^{\perp}\cdot[\mathbf{J}(\mathbf{x}_j-\mathbf{x}_N)]}{|\mathbf{x}_j-\mathbf{x}_N|^2}+\sum_{l=1,\,l\neq j}^{N-1} m_l\frac{\mathbf{x}_j^{\perp}\cdot[\mathbf{J}(\mathbf{x}_j-\mathbf{x}_l)]}{|\mathbf{x}_j-\mathbf{x}_l|^2}\right]$$
$$= \frac{2}{a^2}\left[m_0\frac{\mathbf{x}_j^{\perp}\cdot(\mathbf{J}\mathbf{x}_j)}{|\mathbf{x}_j|^2}+\sum_{l=1,\,l\neq j}^{N-1} m_0\frac{\mathbf{x}_j^{\perp}\cdot(\mathbf{J}\mathbf{x}_j)-\mathbf{x}_j^{\perp}\cdot(\mathbf{J}\mathbf{x}_l)}{|\mathbf{x}_j|^2+|\mathbf{x}_l|^2-2\mathbf{x}_j\cdot\mathbf{x}_l}\right] = \frac{m_0 N}{a^2}$$

for $t\geq 0$. Solving the above ODE and noting that $\beta_N(0)=0$, we obtain $\beta_N(t) = m_0 N t/a^2$ for $t\geq 0$. Thus a combination of the above leads to the solution (2.22). ∎

From the results in Lemma 2.8 we can see that, for the dynamics of (1.11)–(1.12) in Pattern II, the vortex initially at the center of the circle does not move for any time $t\geq 0$, and the other $N-1$ vortices rotate along the circle (counterclockwise if $m_0=+1$ and clockwise if $m_0=-1$) with angular frequency $\omega = N/a^2$ (cf. Figure 14(a),(d)).

LEMMA 2.9. *If the initial data in* (1.12) *are as in Pattern* III*, then the solutions of* (1.11)–(1.12) *are*

$$\mathbf{x}_N(t)\equiv(0,0)^T, \qquad t\geq 0, \tag{2.24}$$

and for $1\leq j\leq N-1$ *with* $N\geq 3$*,*

$$\mathbf{x}_j(t) = a\left(\cos\left(\frac{2j\pi}{N-1}+\theta_0+m_0\omega_N t\right),\,\sin\left(\frac{2j\pi}{N-1}+\theta_0+m_0\omega_N t\right)\right)^T, \tag{2.25}$$

where $\omega_N = (N-4)/a^2$.

The proof is similar to that of Lemma 2.8. From the results in Lemma 2.9, we can see for the dynamics of (1.11)–(1.12) in Pattern III that (i) the vortex initially at the origin does not move during the interaction; (ii) when $N=3$, the two vortices initially located on a circle rotate along the same circle (clockwise if $m_0=+1$ and counterclockwise if $m_0=-1$) with frequency $\omega(a)=1/a^2$ (cf. Figure 15(a)); (iii) the case of $N=4$ is rather special, and the reduced dynamics implies that all four vortices do not move and stay at their initial locations for any $t\geq 0$ (cf. Figure 15(d)); and (iv) when $N\geq 5$, the $N-1$ vortices initially located on a circle rotate along the same circle (counterclockwise if $m_0=+1$ and clockwise if $m_0=-1$) with angular frequency $\omega_N=(N-4)/a^2$ (cf. Figure 15(g)).

LEMMA 2.10. *If the initial data in* (1.12) *satisfy* (2.8)*, i.e., Pattern* IV*, then the solutions of* (1.11)–(1.12) *can be given by*

$$\mathbf{x}_j(t) = \mathbf{x}_j^0 + \frac{m_0}{a}\,t\,(-\sin\theta_0,\,\cos\theta_0)^T, \qquad t\geq 0, \quad j=1,2. \tag{2.26}$$

Proof. From the conservation of the signed mass center (2.4), we have

$$\widetilde{\mathbf{x}}(t) = \frac{\mathbf{x}_1(t)-\mathbf{x}_2(t)}{2} \equiv \frac{\mathbf{x}_1(0)-\mathbf{x}_2(0)}{2} = a\,(\cos\theta_0,\,\sin\theta_0)^T, \quad t\geq 0. \tag{2.27}$$

On the other hand, from the ODEs (1.11), we obtain

$$\frac{d\mathbf{x}_1(t)}{dt} = -2m_0\frac{\mathbf{J}\,(\mathbf{x}_1(t)-\mathbf{x}_2(t))}{|\mathbf{x}_1(t)-\mathbf{x}_2(t)|^2}, \qquad \frac{d\mathbf{x}_2(t)}{dt} = 2m_0\frac{\mathbf{J}\,(\mathbf{x}_2(t)-\mathbf{x}_1(t))}{|\mathbf{x}_2(t)-\mathbf{x}_1(t)|^2}.$$

Summing up the above equations and combining with (2.27), we get

$$\frac{d\mathbf{x}_1(t)}{dt} = -\frac{m_0}{a}\mathbf{J}\,(\cos\theta_0,\,\sin\theta_0)^T, \quad t \geq 0, \quad \text{with} \quad \mathbf{x}_1(0) = \mathbf{x}_1^0. \tag{2.28}$$

Solving (2.28) and noting (2.27), we obtain (2.26) immediately. ∎

From the results in Lemma 2.10 we can see that, for the dynamics of (1.11)–(1.12) in Pattern IV, the two opposite vortices move along two parallel lines which are perpendicular to the line passing through their initial locations with constant velocity (cf. Figures 16(b) and 20(a))

$$\mathbf{v}(t) = \frac{d\mathbf{x}_1(t)}{dt} = \frac{d\mathbf{x}_2(t)}{dt} \equiv \frac{m_0}{a}\,(-\sin\theta_0,\,\cos\theta_0)^T, \qquad t \geq 0. \tag{2.29}$$

3. Numerical results for vortex dynamics in the GLE. In this section, we report the numerical results of the vortex dynamics and interaction by directly simulating the GLE; i.e., we take $\alpha = 1$, $\beta = 0$, $\varepsilon = 1$, and $V(\mathbf{x}) \equiv 1$ in (1.1), with the efficient and accurate time-splitting method introduced in [36]. For the choice of mesh size and time step, as well as the size of the bounded computational domain, we refer to [36]. For comparison, we also exhibit the motion of the vortex centers solved from the reduced dynamics (1.9) in each case. In the figures, the symbols used include + (center of a vortex with index $m = +1$), − (center of a vortex with index $m = -1$), and o (collision position of two or more opposite vortices).

3.1. Interactions of N ($N \geq 2$) like vortices, Patterns I and II. Figure 1 displays the surface plots of $-|\psi|$ at different times when the initial data in (1.7) are chosen as (2.5) with $N = 2$, $m_0 = +1$, and $a = 2$, and Figure 2 shows the time evolution of the vortex centers for different number of vortices $N \geq 2$, i.e., Pattern I. In addition, Figure 3 shows the time evolution of the vortex centers when the initial data in (1.7) is chosen as (2.6)–(2.7) with $m_0 = +1$ and $a = 3$ for different number of vortices $N \geq 3$, i.e., Pattern II.

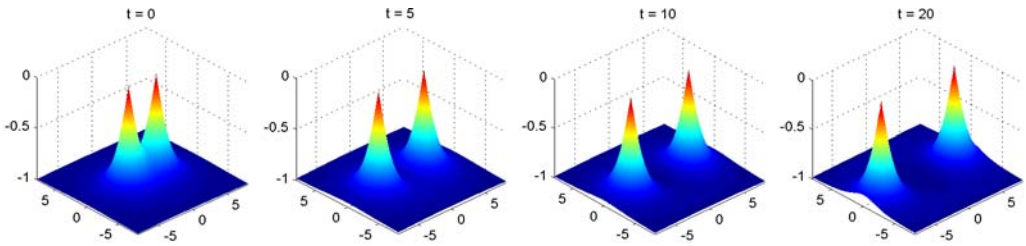

FIG. 1. *Surface plots of* $-|\psi|$ *at different times for the GLE when the initial condition is chosen as Pattern* I *with* $N = 2$, $m_0 = +1$, *and* $a = 2$ *in* (2.5).

From Figures 1–3, and additional numerical experiments not shown here, we can draw the following conclusions for the interaction of N like vortices in the GLE when the initial data are chosen as either Pattern I or II:

(i) The mass center of the vortex centers is conserved for any time $t \geq 0$ (cf. Figures 2 and 3), which confirms the conservation law in (2.3).

(ii) Vortices with the same index undergo a repulsive interaction and they never collide (cf. Figures 1, 2, and 3). Their speeds depend on their distances to the origin, i.e., the larger the distance, the slower the motion (cf. Figures 2 and 3). In addition,

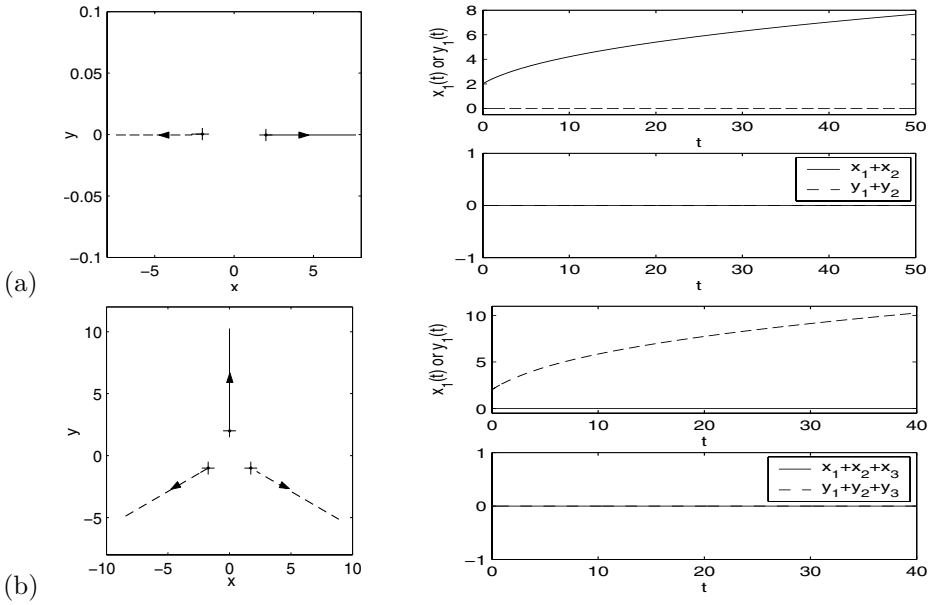

FIG. 2. *Time evolution of vortex centers by directly simulating the GLE when the initial data are chosen as Pattern* I *with* $a = 2$ *and* $m_0 = +1$ *for different* N. (a) $N = 2$; (b) $N = 3$.

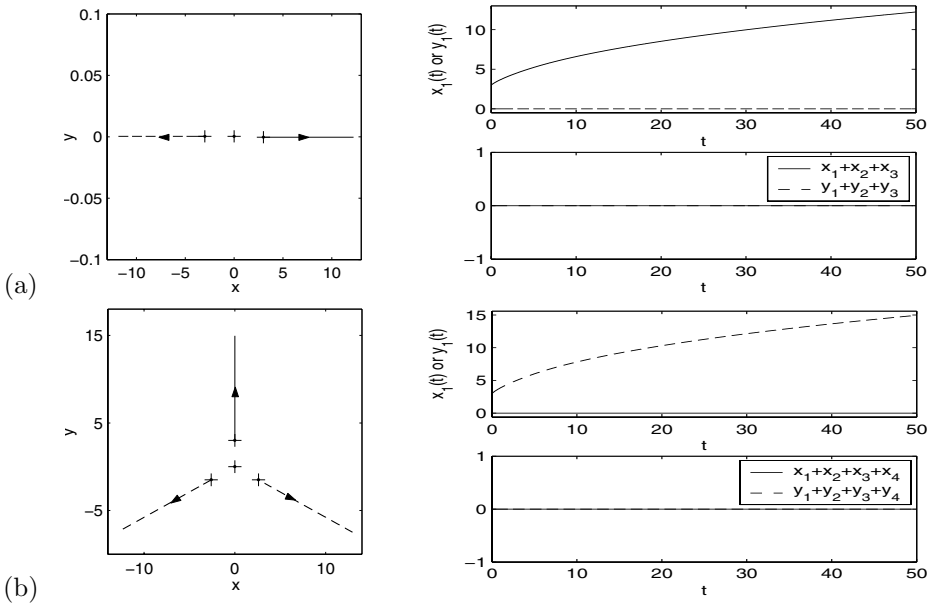

FIG. 3. *Time evolution of vortex centers by directly simulating the GLE when the initial data are chosen as Pattern* II *with* $a = 3$ *and* $m_0 = +1$ *for different* N. (a) $N = 3$; (b) $N = 4$.

in Pattern II the vortex initially at the origin does not move during the dynamics (cf. Figure 3), which confirms the analytical solution (2.12).

(iii) Due to the symmetry of the initial data, the vortices of those initially located on a circle move along lines passing through their initial locations and the origin, and

at any time $t \geq 0$, these vortex centers are always on a circle (cf. Figures 2 and 3), which confirms the analytical solutions (2.9) and (2.13).

(iv) In Patterns I and II, the solutions of the reduced dynamic laws agree qualitatively with our numerical results of the GLE, and quantitatively if a proper κ in (1.9) is chosen, which depends on the initial setup in (1.7). For example, in Pattern I with $N = 2$, we numerically find that the two solutions are the same when we choose $\kappa \approx 2.1279$, 2.1690, 2.2589, and 2.3116 for $a = 4$, 5, 10, and 20, respectively, which suggests that $\frac{1}{\kappa} \approx 0.424 + \frac{0.1897}{a}$ when $a \geq 4$.

3.2. Interactions of N ($N \geq 3$) opposite vortices, Pattern III. Figure 4 shows time evolution of the vortex centers when the initial data in (1.7) are chosen as Pattern III with $m_0 = +1$ and $a = 3$ for different $N \geq 3$.

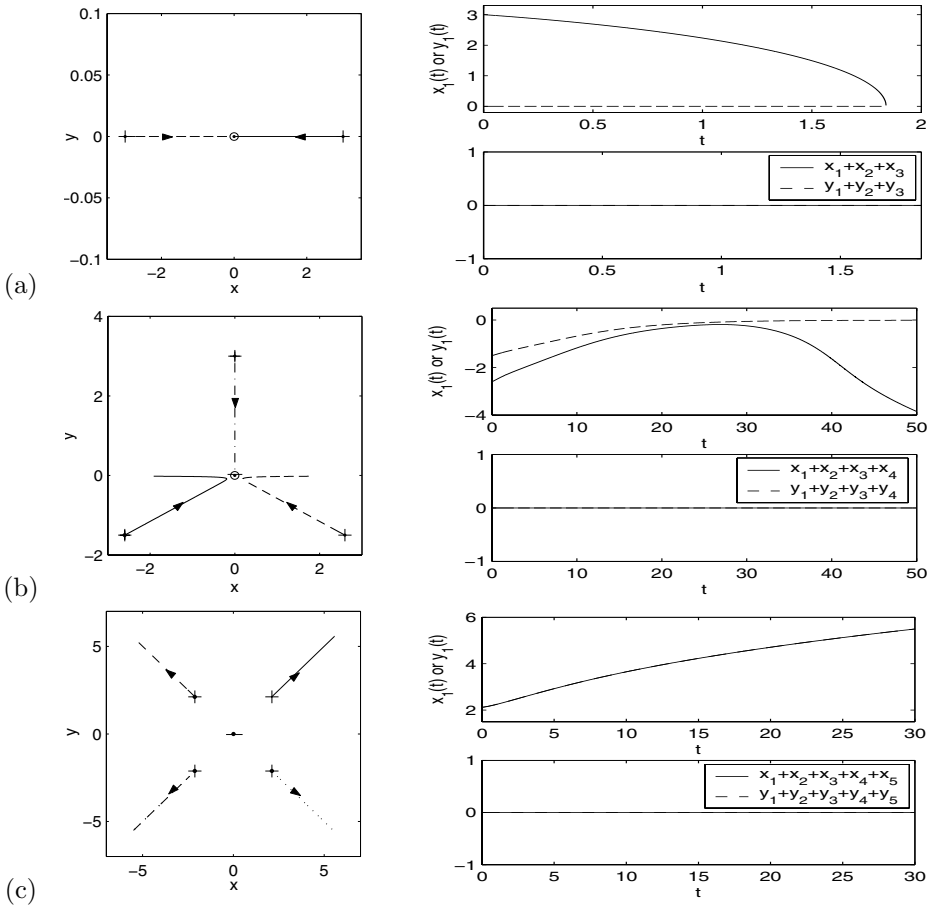

FIG. 4. *Time evolution of vortex centers by directly simulating the GLE when the initial data are chosen as Pattern* III *with* $a = 3$ *and* $m_0 = +1$ *for different* N. (a) $N = 3$; (b) $N = 4$; (c) $N = 5$.

From Figure 4, and additional numerical experiments not shown here, we can draw the following conclusions for the interaction of N opposite vortices in the GLE when the initial data are chosen as Pattern III:

(i) The mass center of the vortex centers is conserved for any time $t \geq 0$ (cf. Figure 4), which confirms the conservation law in (2.3).

(ii) The vortex initially at the origin does not move for any time $t \geq 0$ (cf. Figure 4), which confirms the analytical solution (2.15). The vortices of those initially located on a circle move to the origin when $N = 3$ or 4 and, respectively, move away when $N \geq 5$, along lines passing through their initial location and the origin, and at any time $t \geq 0$, these vortex centers are always on a circle (cf. Figure 4), which confirms the analytical solutions (2.16). Their speeds depend on their distances to the origin, i.e., the larger the distance, the slower the motion.

(iii) When $N = 3$ or 4, collisions between the vortex centers are observed at a critical time t_c (cf. Figure 4(a),(b)). The collision time is quadratically proportional to the initial distance a. Before collision, the interaction is attractive. When $N = 3$, they collide at the origin, and after the collision, there is one vortex with index $m = m_0$ left, and it stays at the origin forever (cf. Figure 4(a)). On the other hand, when $N = 4$, one of the three vortices initially located on the circle collides with the one initially at the origin. After the collision, two like vortices remain and they undergo a repulsive interaction (cf. Figure 4(b)).

(iv) When $N \geq 5$, the vortices undergo repulsive interactions and never collide (cf. Figure 4(c)).

(v) In Pattern III, when $N = 3$ or $N \geq 5$, the solutions of the reduced dynamic laws qualitatively agree with our numerical results of the GLE. On the contrary, they are completely different for $N = 4$. One may argue that a possible cause is the fact that this case corresponds to a degenerate case of the reduced dynamics (1.9)–(1.10) for which the vortices remain stationary, and thus the next order effect becomes important in the underlying vortex motion of the original GLE. In fact, the collision time needed for $N = 4$ ($t_c \approx 28$; cf. Figure 4(b)) is much longer than that for $N = 3$ ($t_c \approx 1.8$; cf. Figure 4(a)) with the same initial radius of the circle at $a = 3$.

3.3. Interactions of two opposite vortices, Pattern IV. Figure 5 displays the surface plots of $-|\psi|$ at different times and Figure 6 shows time evolution of the vortex centers when the initial data in (1.7) are chosen as (2.8) with $m_0 = +1$ and $a = 1.5$, i.e., Pattern IV.

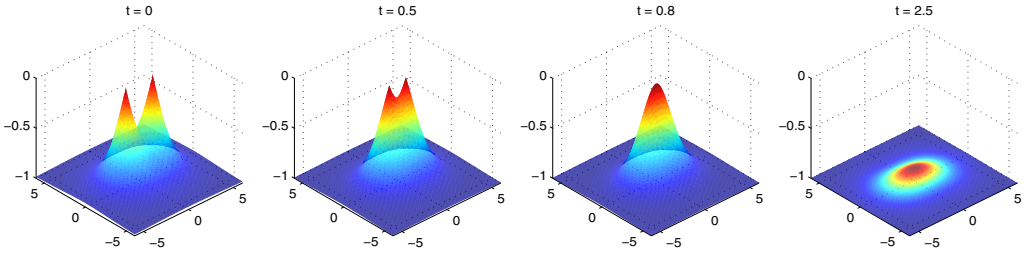

FIG. 5. *Surface plots of* $-|\psi|$ *at different times for the GLE when the initial condition is chosen as Pattern* IV (2.8) *with* $m_0 = +1$ *and* $a = 1.5$.

From Figures 5–6, we can draw the following conclusions for the interaction of two opposite vortices in the GLE when the initial condition is chosen as Pattern IV:

(i) The mass center of the two vortex centers is conserved for any time $t \geq 0$ (cf. Figure 6), which again confirms the conservation law in (2.3).

(ii) Two vortices with opposite winding numbers undergo an attractive interaction (cf. Figure 5), and their centers move along a straight line passing through their locations at $t = 0$ (cf. Figure 6). The speed of the motion for the two vortex

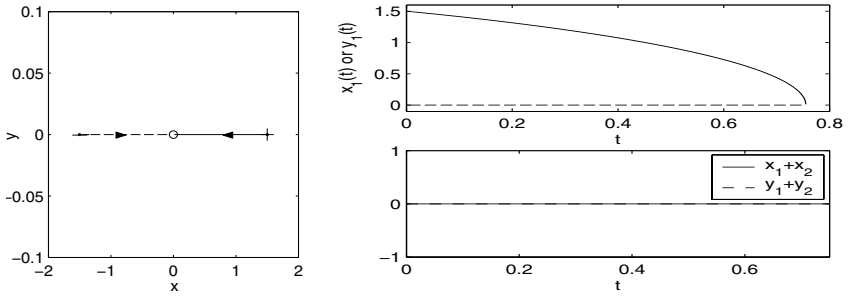

FIG. 6. *Time evolution of vortex centers by directly simulating the GLE when the initial data are chosen as Pattern* IV *with* $a = 1.5$ *and* $m_0 = +1$.

centers depends on their distance. The smaller the distance, the faster the motion (cf. Figure 6).

(iii) There exists a critical time $t_c > 0$, and the two opposite vortices collide with each other at the origin (cf. Figure 5). From our numerical results, we find numerically that the collision time depends on the distance of the two vortex centers at $t = 0$ as

$$t_c \approx \frac{1}{14.8710}\, d_0^{2.0715} \quad \text{with} \quad d_0 = 2a, \qquad a > 0. \tag{3.1}$$

This immediately implies that $t_c = O\left(a^2\right)$, which confirms the analytical result of the collision time in Lemma 2.6.

(iv) Again, in Pattern IV the solutions of the reduced dynamic laws agree qualitatively with our numerical results of the GLE, and quantitatively if a proper κ in (1.9) is chosen, which depends on the initial distance between the two vortex centers.

3.4. Interactions of vortices with nonsymmetric setups. Figures 7–9 show the time evolution of the vortex centers when the initial data in (1.7) are chosen as the three cases in Pattern V, respectively.

Based on Figures 7–9 and our additional numerical experiments, we can draw the following conclusions for three vortices with nonsymmetric initial setups:

(i) When they have the same index, they never collide (cf. Figure 7). On the contrary, when they have opposite indices, they collide at a finite time (cf. Figures 8 and 9), and after collision, only one vortex is left.

(ii) The mass centers of the vortex centers are not conserved (cf. Figures 7–9) during the dynamics within the time frame we computed the solutions, which suggests that there is a considerable discrepancy between the reduced dynamics law (1.9)–(1.10) and the original dynamics in some regimes. One may argue that a possible cause is the fact that the reduced dynamic law is the adiabatic approximation in the leading order when the N vortices are well separated, and thus the next order effect becomes important in the underlying vortex motion of the original GLE when the N vortices are not well separated. In fact, in our numerical results, the larger the distance between the vortex centers, the better the conservation of the mass center (cf. Figures 7–9). This suggests that the reduced dynamics law (1.9)–(1.10) is still a reasonable approximation to the vortex motion of the original GLE in a nonsymmetric initial setup when the N vortices are well separated.

4. Numerical results for vortex dynamics in the NLSE. Similarly, in this section we report the numerical results of the vortex dynamics and interaction by

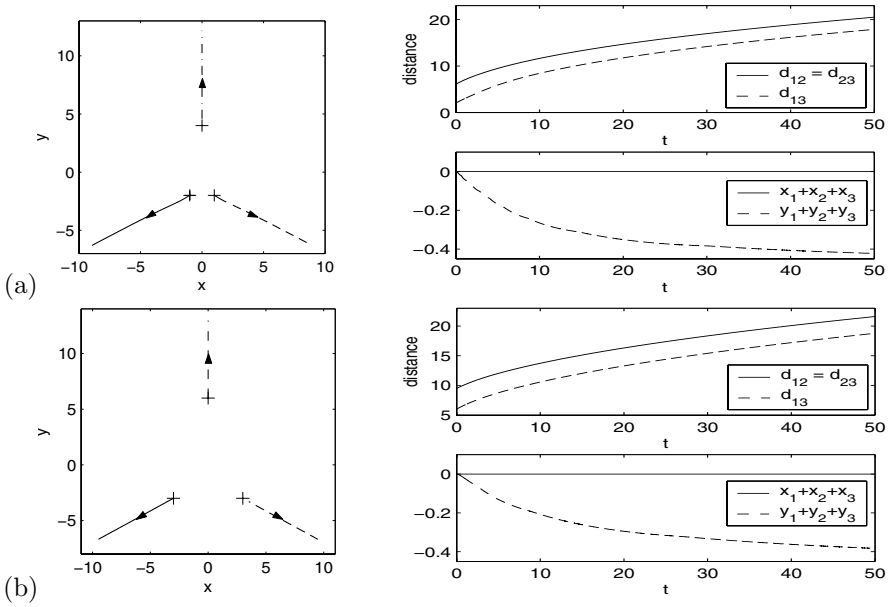

FIG. 7. *Time evolution of vortex centers by directly simulating the GLE when the initial data are chosen as Case* 1 *in Pattern* V *with different* a *and* b. (a) $a = 1$, $b = 4$; (b) $a = 3$, $b = 6$.

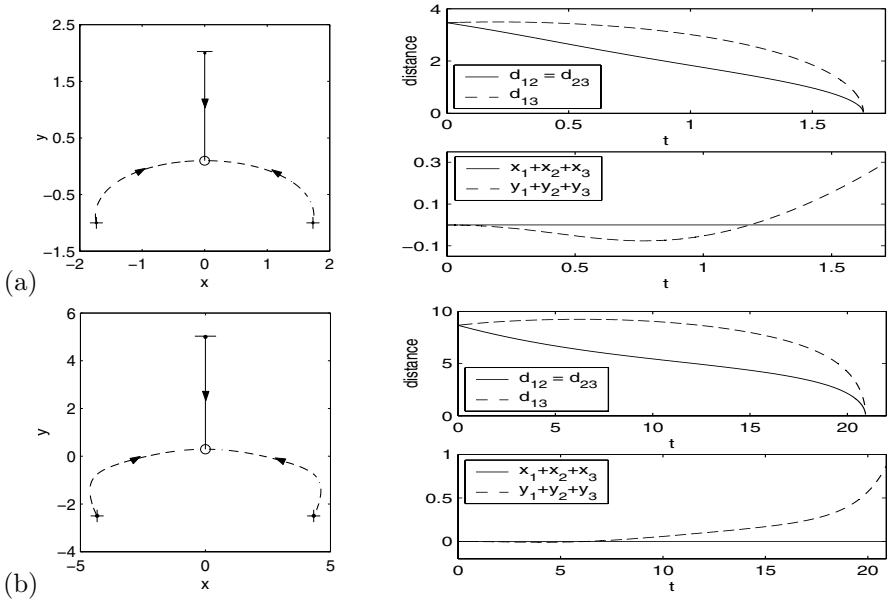

FIG. 8. *Time evolution of vortex centers by directly simulating the GLE when the initial data are chosen as Case* 2 *in Pattern* V *with different* a. (a) $a = 2$; (b) $a = 5$.

directly simulating the nonlinear Schrödinger equation; i.e., we take $\alpha = 0$, $\beta = 1$, $\varepsilon = 1$, and $V(\mathbf{x}) \equiv 1$ in (1.1), with the numerical method introduced in [36]. All the computational setups are the same as in the previous section.

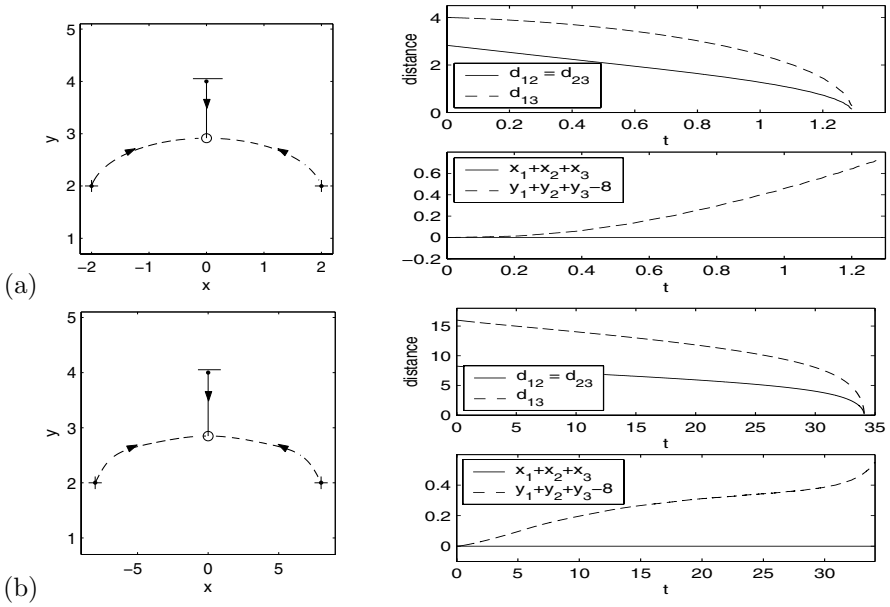

FIG. 9. *Time evolution of vortex centers by directly simulating the GLE when the initial data are chosen as Case* 3 *in Pattern* V *with different* a *and* b. (a) $a = 2$, $b = 4$; (b) $a = 8$, $b = 4$.

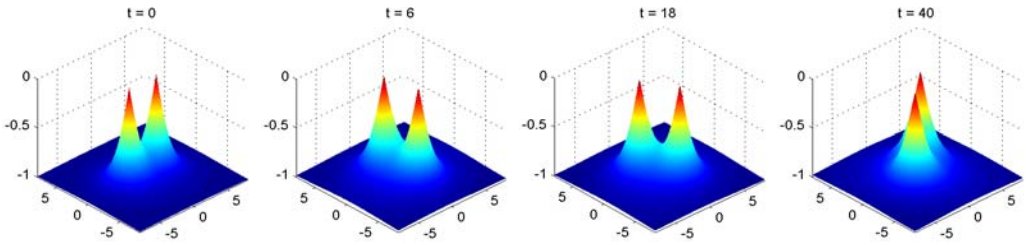

FIG. 10. *Surface plots of* $-|\psi|$ *at different times for the NLSE when the initial condition is chosen as Pattern* I (2.5) *with* $N = 2$, $m_0 = +1$, *and* $a = 2$.

4.1. Interactions of N ($N \geq 2$) like vortices, Patterns I and II. Figures 10–12 give the surface plots of $-|\psi|$ at different times, the slice plots of $|\psi(x, 0, t)|$ at different times, and some dynamical laws when the initial data in (1.7) are chosen as (2.5) with $N = 2$ and $m_0 = +1$, i.e., interaction of two like vortices. In addition, Figure 13 shows time evolution of the vortex centers when the initial condition is chosen as Pattern I (2.5) for different $N \geq 2$, and Figure 14 depicts similar results for Pattern II (2.6)–(2.7).

From Figures 10–14, and additional numerical experiments not shown here, we can draw the following conclusions for the interaction of N like vortices in the NLSE when the initial condition is chosen as either Pattern I or II:

(i) The signed mass center of the vortex centers is conserved for any time $t \geq 0$ (cf. Figures 13(b),(c),(e),(f); 14(b),(c),(e),(f)), which confirms the conservation law in (2.4).

(ii) Vortices with the same index behave like point vortices in an ideal fluid and never collide (cf. Figures 10, 13, and 14). In fact, there exists a critical time $t_0 > 0$,

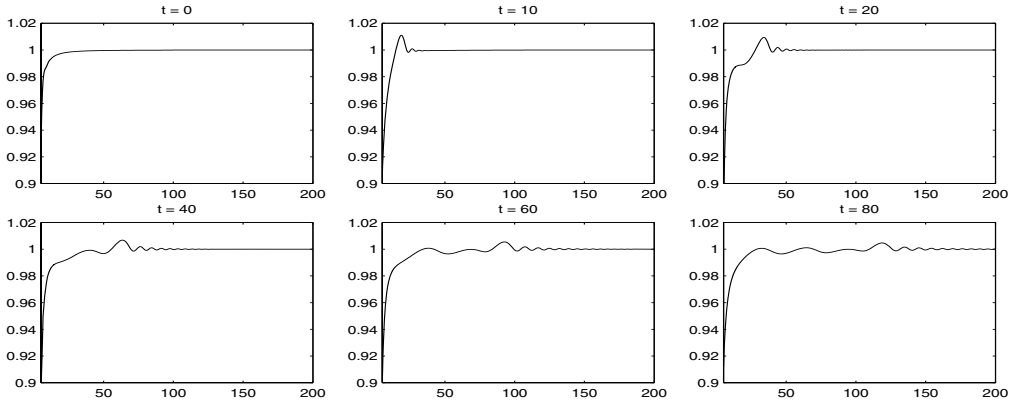

FIG. 11. *Plots of* $|\psi(x,0,t)|$ $(x \geq 4)$ *at different times for the NLSE when the initial condition is chosen as Pattern* I (2.5) *with* $N = 2$, $m_0 = +1$, *and* $a = 2$, *showing the sound wave propagation.*

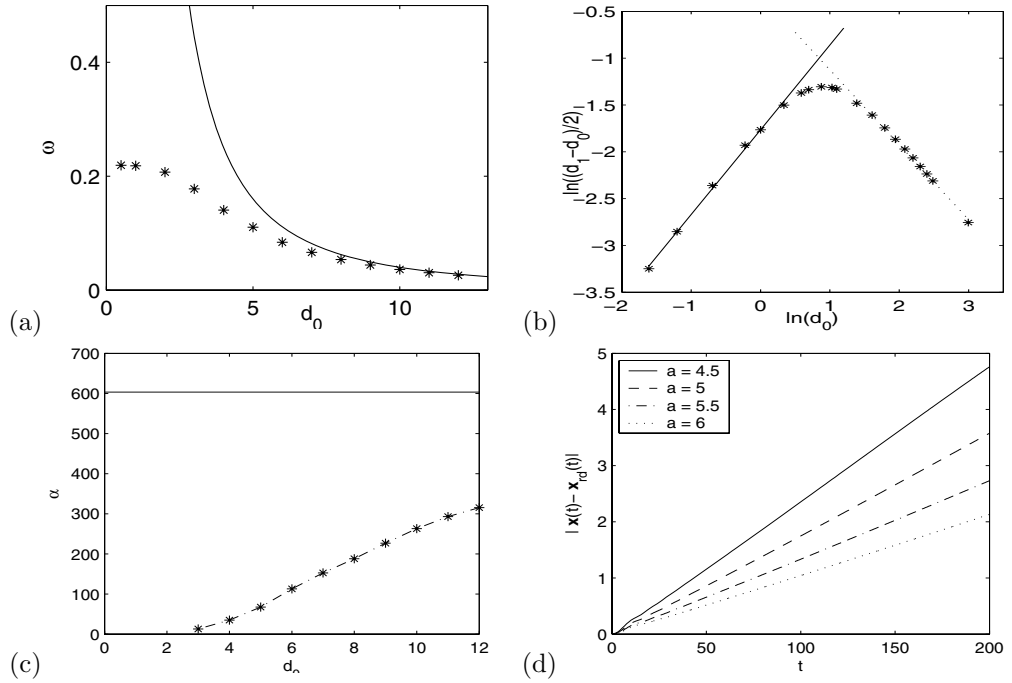

FIG. 12. *Dynamical laws of interaction between two like vortices, i.e., Pattern* I *with* $N = 2$, *in the NLSE.* (a) *Frequency* ω *of the rotation (solid line is from* (2.18) *and asterisks are our numerical results);* (b) *diameter* $d_1 = |\mathbf{x}_1(t_0) - \mathbf{x}_2(t_0)|$ *when the two vortices start to rotate on a circle;* (c) $\alpha(d_0)$ *in* (4.1) (*the asterisks are our numerical results and the solid line is from the theoretical predication* $\alpha = 2^6 \cdot 3\pi$ [30]); (d) *errors of the vortex centers between the solution* (2.18) *of the reduced dynamic laws* (*denoted* $\mathbf{x}_{\rm rd}(t)$) *and our directly simulating results of the NLSE* (*denoted* $\mathbf{x}(t)$) *for different initial distance* $d_0 = 2a$.

depending on the initial distance to the origin, i.e., a, such that before time t_0, i.e., when $0 \leq t \leq t_0$, the vortices initially located on a circle move from their initial locations to another circle, and the change in distance between each vortex to the origin is rapid (cf. Figures 13(b), 14(b)); after time t_0, i.e., for $t \geq t_0$, the vortices

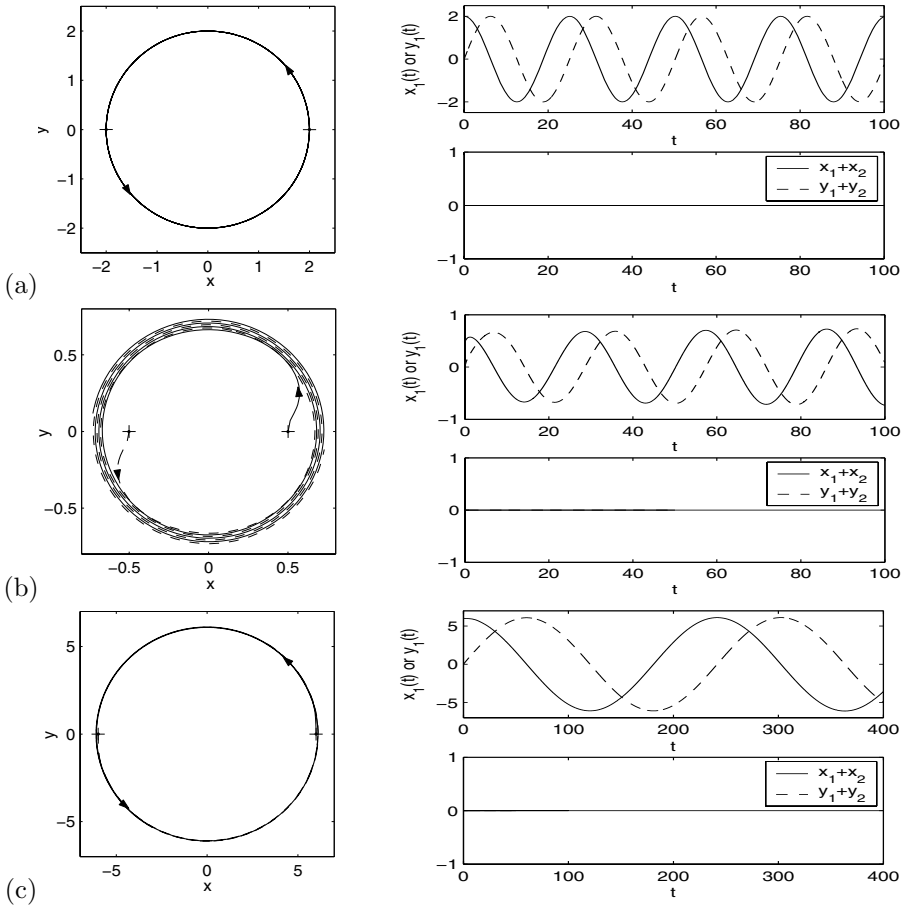

FIG. 13. *Time evolution of vortex centers for the NLSE when the initial condition is chosen as Pattern* I *with different* N. (a) *and* (d) *are from the reduced dynamic laws* (2.18)*;* (b) *and* (e) *and* (c) *and* (f) *show direct simulation results of the NLSE with* $a = O(r_1^0)$ *and* $a \gg r_1^0$*, respectively. Case* 1: $N = 2$ *with* (b) $a = 0.5$ *and* (c) $a = 6$.

rotate uniformly along a circle (counterclockwise when winding number $m_0 = +1$ and clockwise when $m_0 = -1$) with angular frequency ω depending on a and the radius of the circle increasing very slowly. The sound wave propagation is clearly observed during the interaction (cf. Figure 11). In addition, in Pattern II, the vortex initially at the origin does not move during the dynamics (cf. Figure 14(b),(c),(e),(f)), which confirms the analytical solution (2.21).

(iii) For Pattern I with $N = 2$, we also present the comparison quantitatively (cf. Figure 12). In this case, denote $d_0 = |\mathbf{x}_1^0 - \mathbf{x}_2^0| = 2a$ and $d_1 = |\mathbf{x}_1(t_0) - \mathbf{x}_2(t_0)|$ for the initial distance and the diameter of the circle at time $t = t_0$ of the two vortices, respectively. The angular frequency predicted by the reduced dynamics is confirmed by our numerical simulations (cf. Figure 12(a)) when $d_0 = 2a$ is large, and it is invalid when d_0 is small; i.e., the reduced dynamics is invalid when the vortex pair initially has overlapping support. Furthermore, even when the two vortices are well separated, the reduced dynamics fails to take into account the effect of the excessive energy and the radiation, which play important roles in the NLSE vortex dynamics. For example,

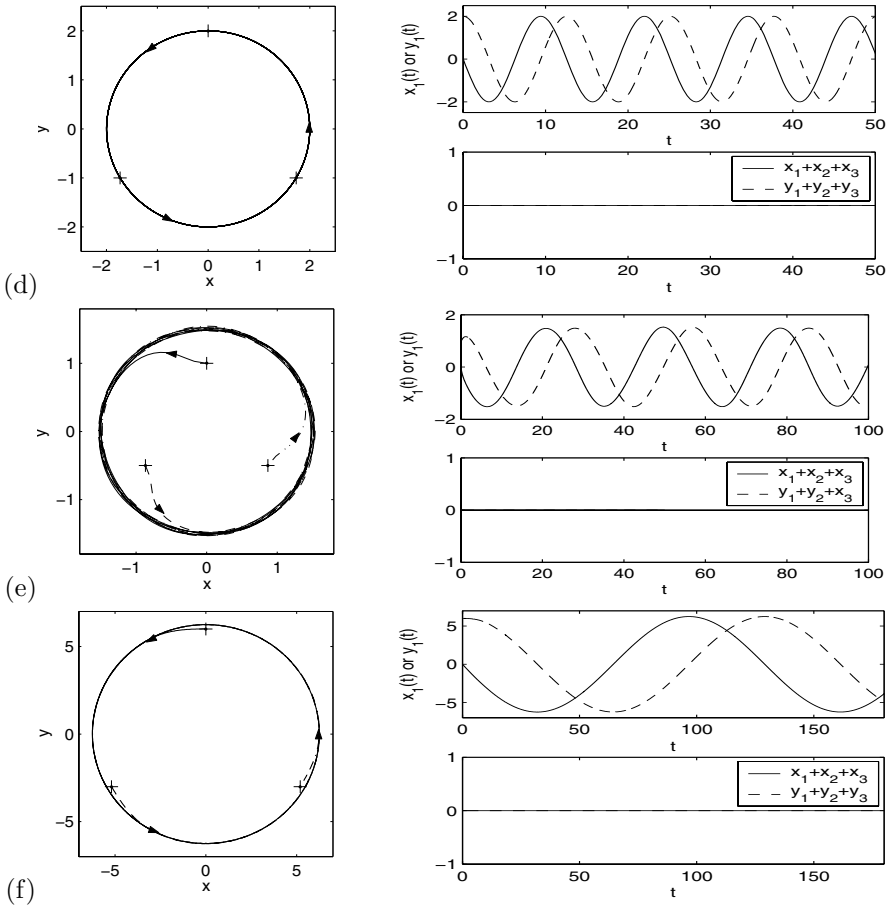

FIG. 13 (*cont.*). *Case* 2: $N = 3$ *with* (e) $a = 1$ *and* (f) $a = 6$.

by analyzing the next-order approximation for the interaction of two well-separated vortices in the NLSE, it was derived in [30] that the diameter of the circle increases on the order of $O(t^{1/6})$, i.e., asymptotically,

$$d(t) = |\mathbf{x}_1(t) - \mathbf{x}_2(t)| = \left(|\mathbf{x}_1^0 - \mathbf{x}_2^0|^6 + 2^6 \cdot 3\pi t\right)^{1/6} = \left(d_0^6 + 2^6 \cdot 3\pi t\right)^{1/6}. \tag{4.1}$$

This departs from the constant distance prediction made from the reduced dynamic laws (1.11). Numerically, we fit the distance between the two vortex centers $d(t) = |\mathbf{x}_1(t) - \mathbf{x}_2(t)|$ for $t \geq t_0$ by

$$d(t) = |\mathbf{x}_1(t) - \mathbf{x}_2(t)| = \left(d(t_0)^6 + \alpha(d_0)(t - t_0)\right)^{1/6}, \qquad t \geq t_0, \tag{4.2}$$

with $\alpha(d_0)$ being a constant depending on d_0. The results show that (4.1) is a very good prediction (cf. Figure 12(c)). Of course, much more detailed information on the vortex dynamics in the NLSE can be found through our numerical simulations. For example, our simulations suggest that when the initial distance between the two vortex centers increases, the time t_0 increases, the diameter $d_1 = d(t_0)$ of the circle at $t = t_0$ increases (cf. Figure 12(b)), and $\alpha(d_0)$ in (4.2) increases (cf. Figure 12(c)). From Fig-

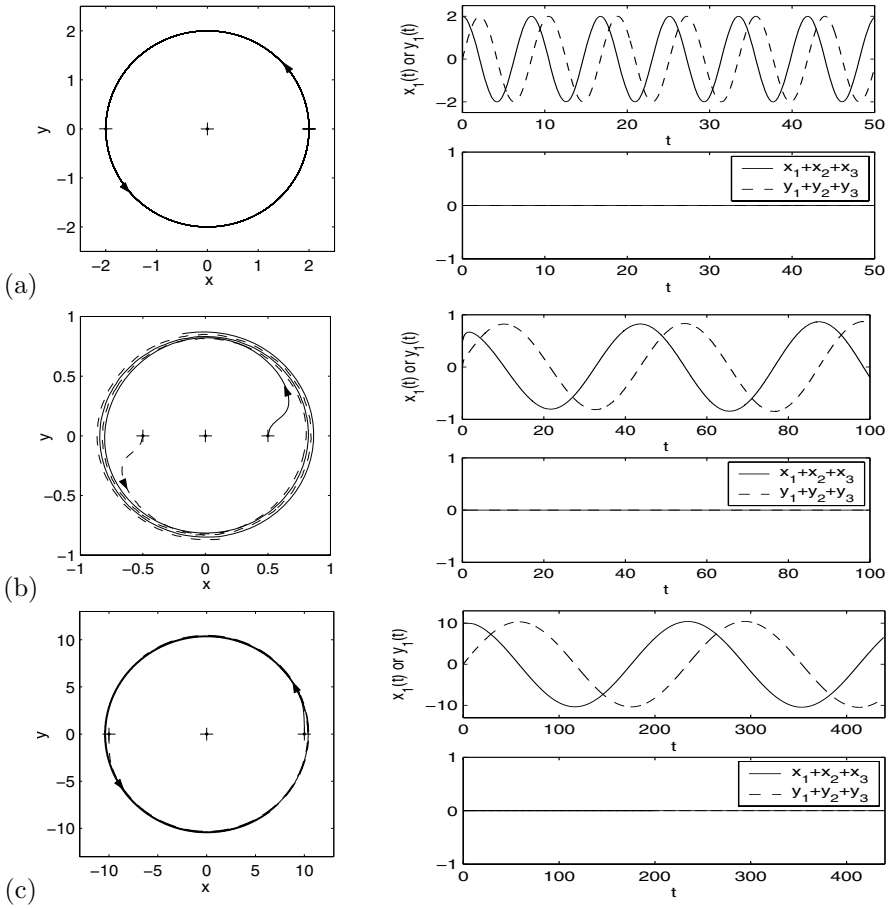

FIG. 14. *Time evolution of vortex centers for the NLSE when the initial condition is chosen as Pattern* II *with different* N. (a) *and* (d) *are from the reduced dynamic laws* (2.21)–(2.22)*;* (b) *and* (e) *and* (c) *and* (f) *show direct simulation results of the NLSE with* $a = O(r_1^0)$ *and* $a \gg r_1^0$*, respectively. Case* 1: $N = 3$ *with* (b) $a = 0.5$ *and* (c) $a = 10$.

ure 12(b), we have the numerical dynamical laws for the diameter d_1 for different d_0:

$$d_1 := d(t_0) \approx \begin{cases} d_0 + d_0^{0.9053}/2.9189, & d_0 < r_1^0, \\ d_0 + 1.4453/d_0^{0.7996}, & d_0 > 2r_1^0, \end{cases}$$

where $r_1^0 \approx 1.75$ [36] is the core size for the vortex state ϕ_m in (1.4) of the GLSE with winding number $m = \pm 1$.

(iv) In Patterns I and II, the solutions of the reduced dynamic laws agree qualitatively with our numerical results of the NLSE, and quantitatively when time t is small and they are well separated, i.e., $a \gg r_1^0 = 1.75$ [36]. In general, for a fixed initial distance, i.e., a, the error increases when time increases; for a given time, the error decreases when the initial distance increases (cf. Figure 12(d)). This again suggests that the reduced dynamics for governing time evolution of the vortex centers in the NLSE is valid only when time t is small and the initial distance is very large. Corrections must be added, e.g., such as (4.1), when either the time t is large or the initial distance is not very large.

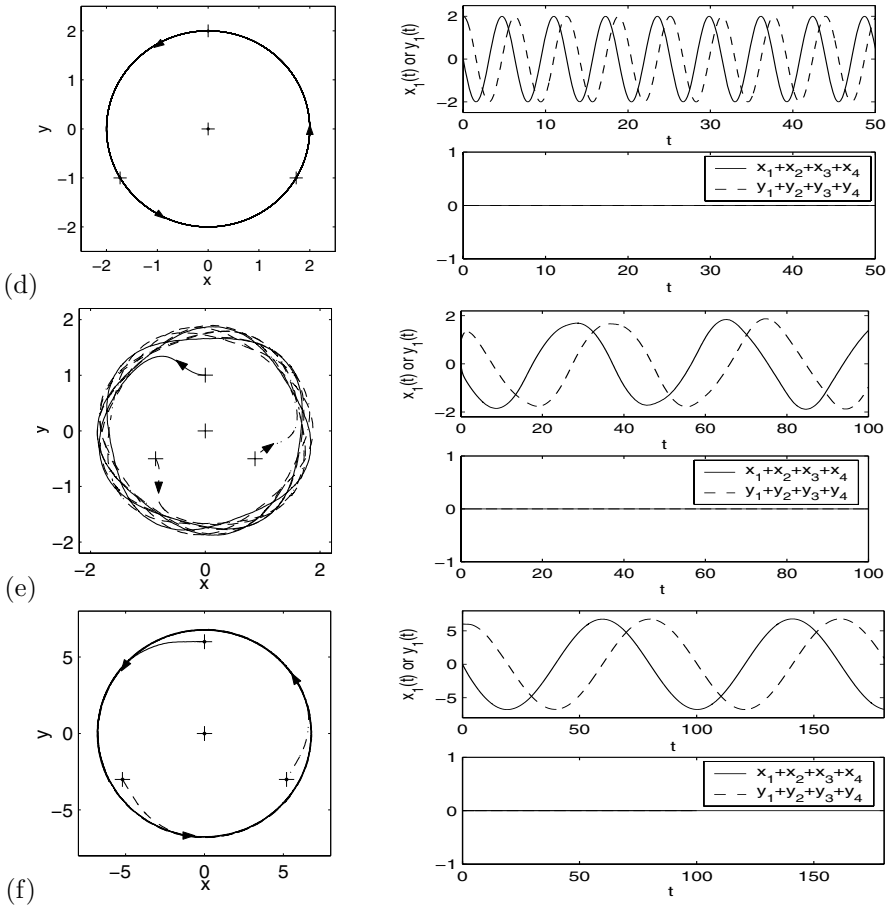

FIG. 14 (*cont.*). *Case* 2: $N = 4$ *with* (e) $a = 1$ *and* (f) $a = 6$.

(v) The results in Figure 12, as well as in Figure 21, also confirm Kirchoff's laws rigorously derived in [23, 24] for the interaction of two vortices in the NLSE, i.e., $\alpha = 0$, $\beta = 1$, $V(\mathbf{x}) \equiv 1$ in (1.1), when $\varepsilon \to 0$ with the initial distance between the two vortex centers fixed. In fact, the vortex interactions of (1.1) with $V(\mathbf{x}) \equiv 1$, $\varepsilon = 1$, and increased initial distances between the vortex centers are equivalent to those of (1.1) with $V(\mathbf{x}) \equiv 1$, $\varepsilon \to 0$, and fixed initial distances between the vortex centers by applying a rescaling.

4.2. Interactions of N ($N \geq 3$) opposite vortices, Pattern III. Figure 15 shows the time evolution of the vortex centers for different $N \geq 3$ when the initial data in (1.7) are chosen as in Pattern III with $m_0 = +1$ for different N and a.

From Figure 15, and additional numerical experiments not shown here, we can draw the following conclusions for the interaction of N opposite vortices in the NLSE when the initial data are chosen as Pattern III:

(i) The signed mass center of the vortex centers is conserved for any time $t \geq 0$ (cf. Figure 15(b),(c),(e),(f),(h),(i)), which confirms the conservation law in (2.4).

(ii) The vortex initially at the origin does not move for any time $t \geq 0$ (cf. Figure 15(b),(c),(e),(f),(h),(i)), which confirms the analytical solution (2.24). After a critical

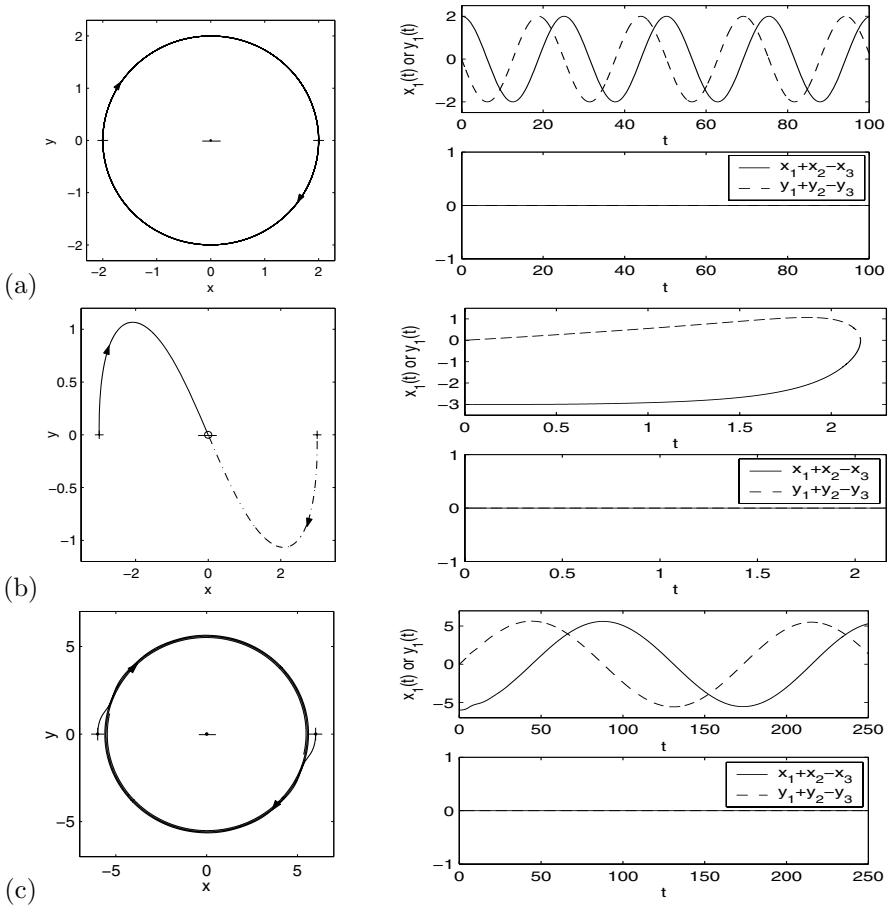

FIG. 15. *Time evolution of vortex centers for the NLSE when the initial condition is chosen as Pattern* III *with different* N *and* a. (a), (d), *and* (g) *are from the reduced dynamic laws* (2.25); (b), (e), *and* (h) *and* (c), (f), *and* (i) *show direct simulation results of the NLSE with* $a = O(r_1^0)$ *and* $a \gg r_1^0$, *respectively. Case* 1: $N = 3$ *with* (b) $a = 3$ *and* (c) $a = 6$.

time t_c depending on the initial radius a, the vortices initially located on a circle rotate clockwise when $N = 3$ and $a > a_{\rm cr} \approx 2r_1^0$ or $N = 4$, and, respectively, counterclockwise when $N \geq 5$, along a circle, and at any time $t \geq 0$, these vortex centers are always on a circle (cf. Figure 15(b),(c),(e),(f),(h),(i)), which confirms the analytical solutions (2.25). Their angular frequencies depend on their distances to the origin, i.e., the larger the distance, the slower the motion.

(iii) For the case of $N = 3$, when the initial radius $a < 2r_1^0$, the three vortices undergo attractive interactions, and the two vortices initially on a circle move symmetrically towards the center before a critical time t_c. When $t = t_c$, they collide at the origin (cf. Figure 15(b)), and after it, only one vortex with a winding number m_0 is left and stays at the point $(0, 0)$ for any time $t > t_c$. On the other hand, when $a > 2r_1^0$, the two vortices rotate (clockwise for $m_0 = +1$, and, respectively, counterclockwise for $m_0 = -1$) on a circle whose radius increases very slowly with time t (cf. Figure 15(c)).

(iv) When $N = 4$, the three vortices initially on a circle move to another circle

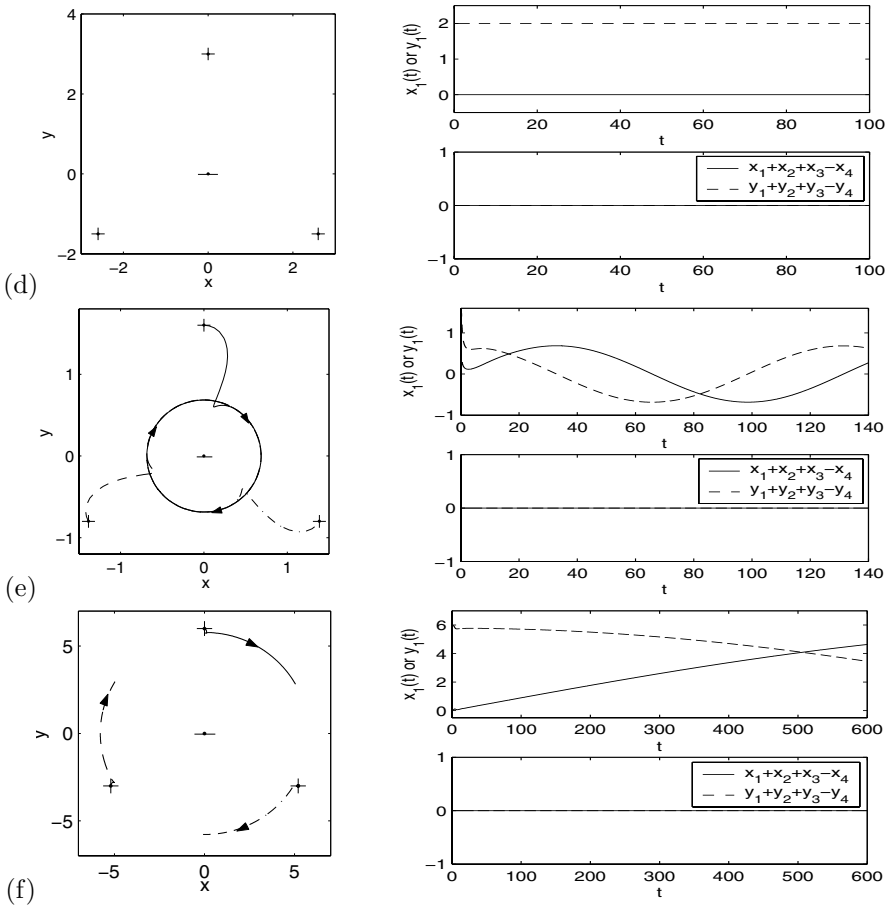

FIG. 15 (*cont.*). *Case* 2: $N = 4$ *with* (e) $a = 1.6$ *and* (f) $a = 6$.

with radius $a_1 < a$; then they rotate (clockwise for $m_0 = +1$, and, respectively, counterclockwise for $m_0 = -1$) on a circle whose radius increases very slowly with time t (cf. Figure 15(e),(f)). The four vortices never collide no matter how small a is.

(v) When $N \geq 5$, the $N-1$ vortices initially on a circle move to another circle with radius $a_1 > 0$; then they rotate (counterclockwise for $m_0 = +1$, and, respectively, clockwise for $m_0 = -1$) on a circle whose radius increases very slowly with time t (cf. Figure 15(h),(i)).

(vi) In Pattern III, when $N = 3$ and $a > 2r_1^0$ or $N \geq 5$, the solutions of the reduced dynamic laws agree qualitatively with our numerical results of the NLSE. On the contrary, when $N = 4$ or $N = 3$ with $a < 2r_1^0$, they are completely different! This may be attributed to the lack of well separation between the vortex cores and/or the next-order effect in the underlying vortex motion of the original NLSE. In fact, the angular frequency for $N = 4$ is much larger than that for $N = 3$ with the same initial radius of the circle (cf. Figure 15(c),(f)).

4.3. Interactions of two opposite vortices, Pattern IV. Figure 16 displays the surface plots of $-|\psi|$ at different times when the initial data in (1.7) are chosen as (2.8), i.e., Pattern IV, with $m_0 = +1$ and $a = 1.5$ or $a = 5$. Figures 17 and 18–19 plot $|\psi(x, y(t), t)|$ and $|\psi(0, y, t)|$, respectively, to show the sound wave propagation

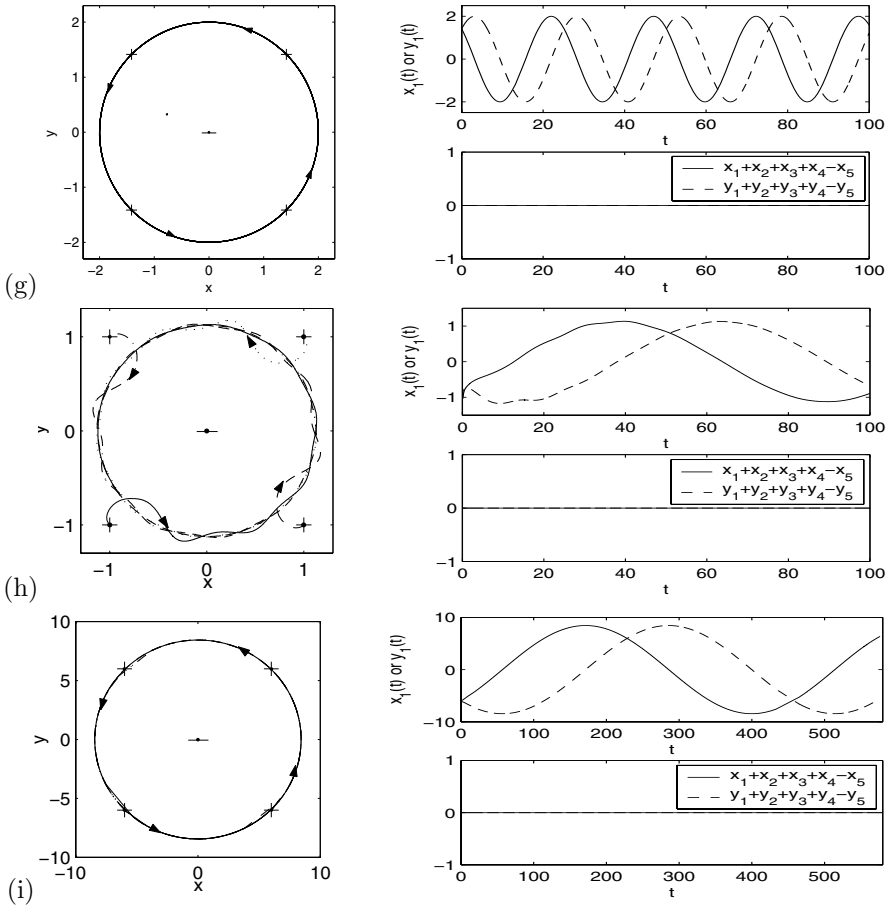

FIG. 15 (*cont.*). *Case* 3: $N = 5$ *with* (h) $a = 1$ *and* (i) $a = 6$.

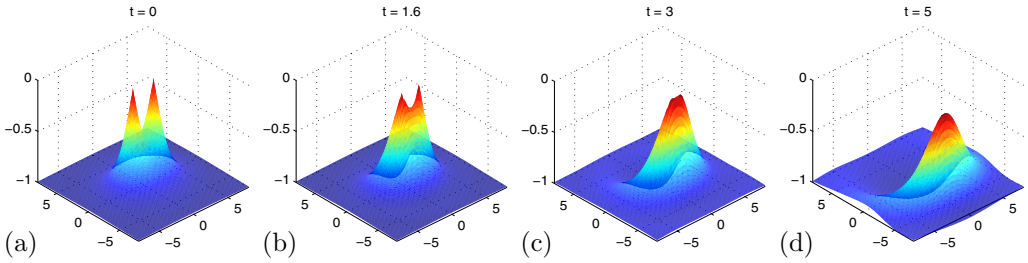

FIG. 16. *Surface plots of* $-|\psi|$ *at different times for the NLSE when the initial condition is chosen as Pattern* IV (2.8) *with* $m_0 = +1$. I. $a = 1.5 = O(r_1^0)$.

during the dynamics. Figure 20 shows the time evolution of the two vortex centers with different $d_0 = 2a$. In addition, Figure 21 shows some dynamical laws for the interaction.

From Figures 16–21, we can draw the following conclusions for the interaction of two opposite vortices in the NLSE when the initial condition is chosen as Pattern IV:

(i) The signed mass center of the two vortex centers is not conserved, at least when either the initial distance between the two vortices is not large or time t is small

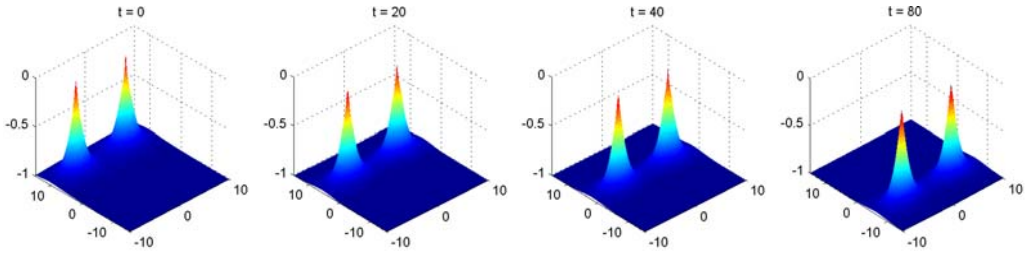

FIG. 16 (*cont.*). II. $a = 5 \gg r_1^0$.

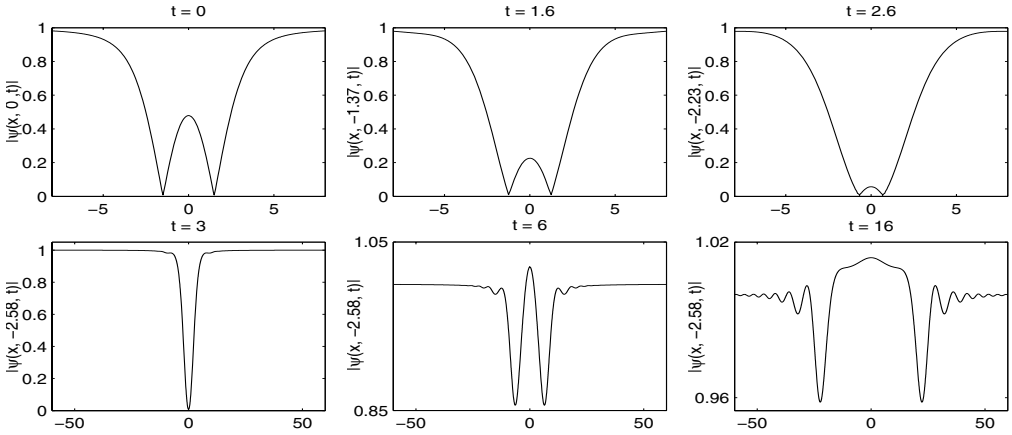

FIG. 17. *Plots of* $|\psi(x, y(t), t)|$ *at different times for the NLSE when the initial condition is chosen as Pattern* IV (2.8) *with* $m_0 = +1$ *and* $a = 1.5$*, showing sound wave propagation and radiation with the values of* $y(t)$ *given in the labels. Here* $y = y(t)$ *is the line passing through the two vortex centers at time* t *before they merge with each other around* $t_c \approx 3.0$.

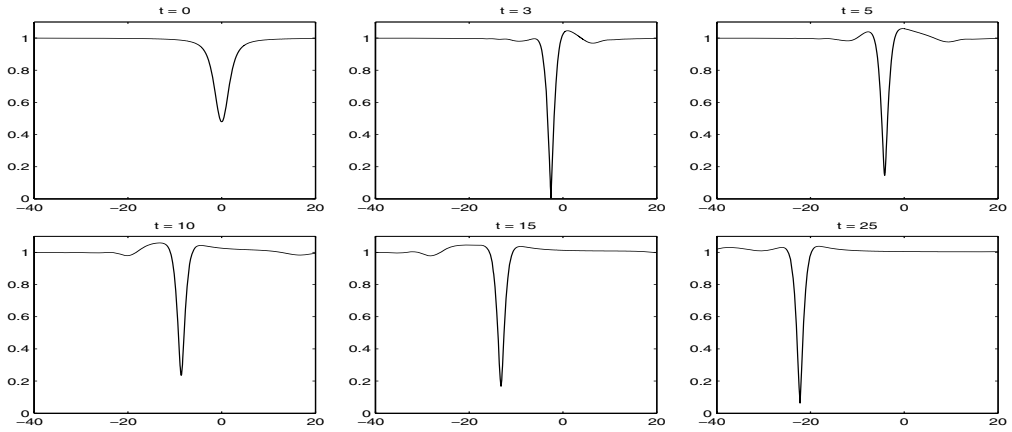

FIG. 18. *Plots of* $|\psi(0, y, t)|$ *at different times for the NLSE when the initial condition is chosen as Pattern* IV (2.8) *with* $m_0 = +1$ *and* $a = 1.5$*, showing solitary-like wave propagation.*

(cf. Figure 20(b),(c),(d)), which suggests that the conservation law in (2.4) is invalid when the initial distance between the two vortex centers at time $t = 0$ is not large.

(ii) There is a critical distance $d_{\rm cr}$ satisfying that, for $d_0 = |\mathbf{x}_1^0 - \mathbf{x}_2^0| < d_{\rm cr}$, the

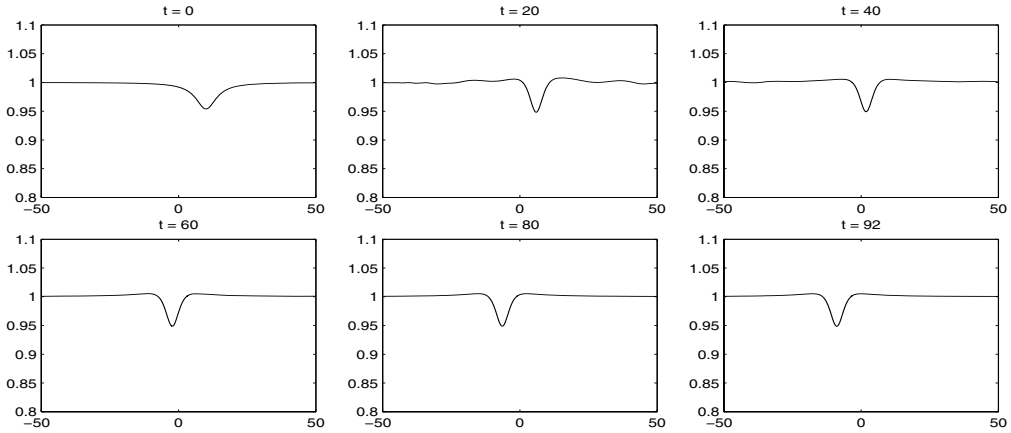

FIG. 19. *Plots of* $|\psi(0, y, t)|$ *at different times for the NLSE when the initial condition is chosen as Pattern* IV (2.8) *with* $m_0 = +1$ *and* $a = 5 \gg r_1^0$ *for solitary wave propagation.*

two vortices approach each other while drifting sideways and then collide and are annihilated at time $t = t_c$ (cf. Figures 16, 20(b)), and for $d_0 = |\mathbf{x}_1^0 - \mathbf{x}_2^0| > d_{cr}$, they move almost in a parallel course, perpendicular to the line joining them (cf. Figures 19, 20(c),(d)). Our numerical simulations suggest that $d_{\rm cr} \approx 2r_1^0 = 2 \times 1.75 = 3.5$, i.e., double the size of the core size r_1^0, which is almost triple the size of the theoretical prediction $d_{\rm cr} \approx \sqrt{2}$ derived in [30].

(iii) When $d_0 < d_{\rm cr} = 2r_1^0$, before collision, our numerical simulation reveals that two sound waves moving towards each other are generated along the line joining the centers of the two vortices (cf. Figure 17), which cause the collision, while no radiation is observed; after the collision, some outgoing radiation is observed along with a solitary-like sound wave also being observed in the y-axis (cf. Figure 18). In addition, a discontinuity or shock wave in the hydrodynamic velocity is observed just after the collision. Furthermore, for the initial setup in Pattern IV, the two vortices collide at the point $(0, -d_2)$ with $d_2 > 0$ when $t = t_c$. When the initial distance d_0 increases, both t_c and d_2 increase, and our numerical results suggest the following relation between them:

$$t_c \approx \frac{1}{7.0790}\, d_0^{2.0954}, \qquad d_1 \approx \frac{1}{1.9300}\, d_0^{1.0365}, \quad \text{with} \quad d_1 = \sqrt{d_0^2 + d_2^2}.$$

(iv) When $d_0 \gg d_{\rm cr} = 2r_1^0$, the two vortices drift almost on two parallel lines, perpendicular to the line joining them with a constant speed. Our numerical results confirm the speed (2.29) when $d_0 = 2a$ is large (cf. Figure 21(a)). In addition, a solitary wave is observed during the dynamics (cf. Figure 19).

(v) Again, in Pattern IV the solutions of the reduced dynamic laws agree qualitatively with our numerical results of the NLSE when $a \gg r_1^0$ and they are completely invalid when a is small (cf. Figure 20). When $a > r_1^0$, in general, for a fixed initial distance, the error increases when time increases; for a given time, the error decreases when the initial distance increases (cf. Figure 21(b)).

4.4. Interactions of vortices with nonsymmetric setups. Figures 22–24 show time evolution of the vortex centers when the initial data in (1.7) are chosen as the three cases in Pattern V, respectively.

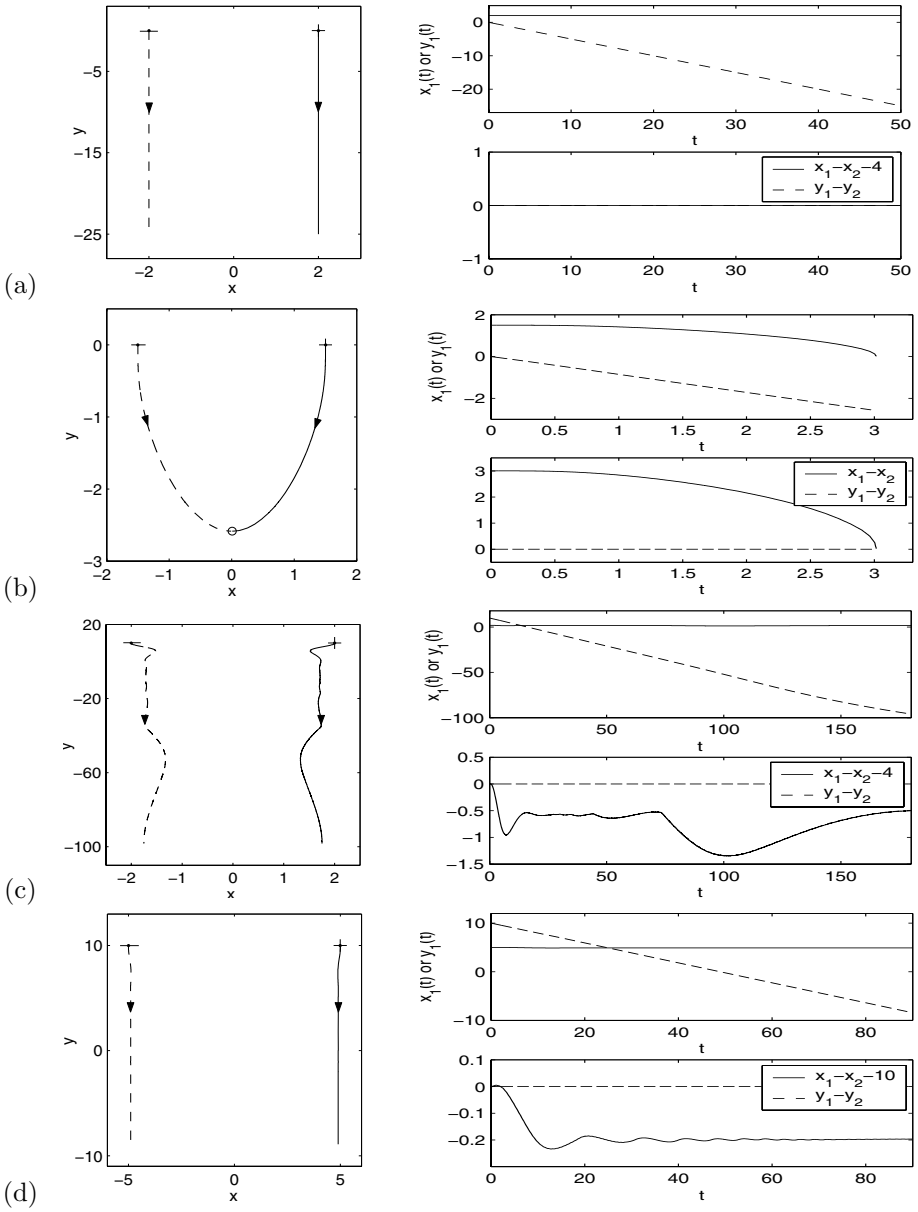

FIG. 20. *Time evolution of vortex centers for the NLSE when the initial condition is chosen as Pattern* IV. (a) *is from the reduced dynamic laws* (2.26)*, and* (b), (c)*, and* (d) *show direct simulation results of the NLSE with* $m_0 = +1$ *and* $a = 1.5 < r_1^0$*,* $a = 2 > r_1^0$*, and* $a = 5 \gg r_1^0$*, respectively.*

Based on Figures 22–24 and our additional numerical experiments, we can draw the following conclusions for three vortices with nonsymmetric initial setups:

(i) When they have the same index, they rotate and never collide (cf. Figure 22). On the contrary, when they have opposite indices, there exists a critical distance $d_{\rm cr}$, when their initial distances are less than $d_{\rm cr}$, they collide at finite time (cf. Figures 23(a), 24(a)), and after collision, only one vortex is left; on the other hand, when their

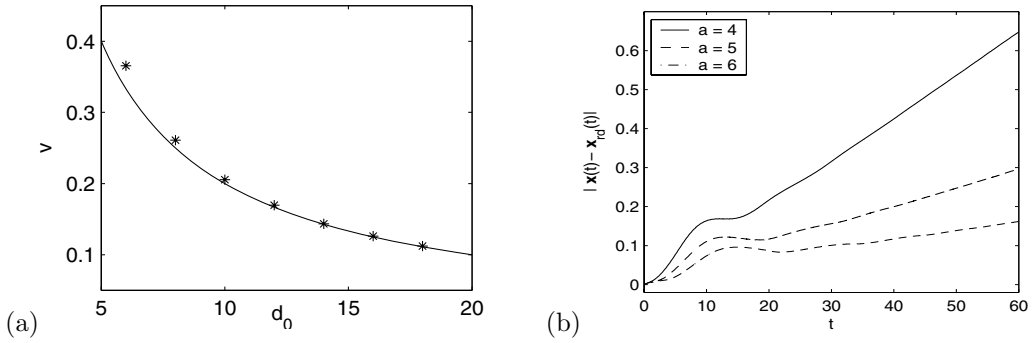

FIG. 21. *Dynamic laws for two opposite vortices, i.e., Pattern* IV *with* $N = 2$*, in the NLSE.* (a) *Speed* v *of the parallel motion.* (b) *Errors of the vortex centers between the solution* (2.26) *of the reduced dynamic laws* (*denoted as* $\mathbf{x}_{\rm rd}(t)$) *and our directly simulating results of the NLSE* (*denoted as* $\mathbf{x}(t)$) *for different initial distance* $d_0 = 2a$.

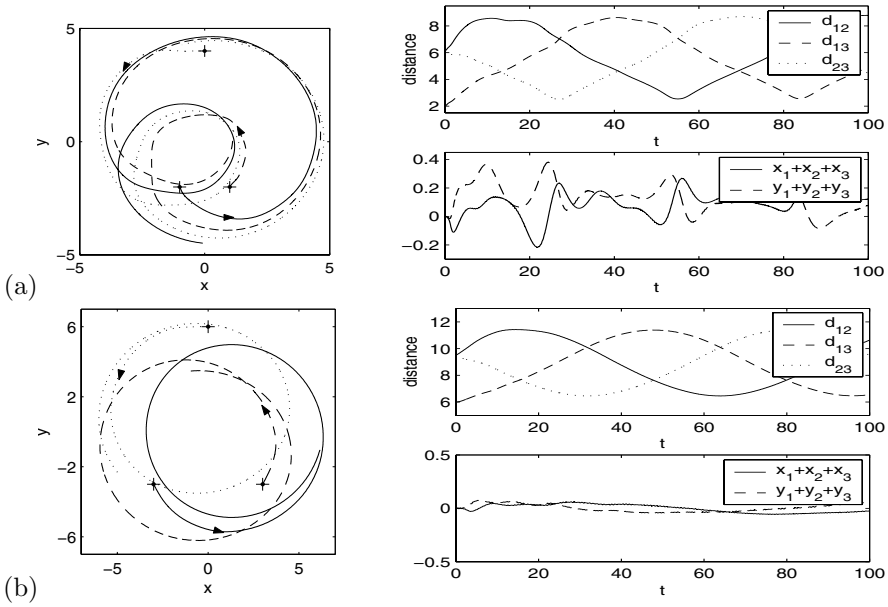

FIG. 22. *Time evolution of vortex centers for the NLSE when the initial condition is chosen as Case* 1 *in Pattern* V *with different* a *and* b. (a) $a = 1$, $b = 4$. (b) $a = 3$, $b = 6$.

initial distances are larger than $d_{\rm cr}$, two of them move in a parallel course and never collide (cf. Figures 23(b), 24(b)).

(ii) The signed mass centers of the vortex centers are not conserved (cf. Figures 22–24) during the dynamics, and these suggest that the reduced dynamics law (1.11)–(1.12) has considerable discrepancy in some regimes. Again, one may argue that a possible cause is the fact that the reduced dynamic law is the adiabatic approximation in the leading order when the N vortices are well separated, and thus the next-order effect becomes important in the underlying vortex motion of the original NLSE when the N vortices are not well separated. Also in our numerical results, the larger the distance between the vortex centers, the better the conservation of the signed mass center (cf. Figures 22–24). This again suggests that the reduced dynam-

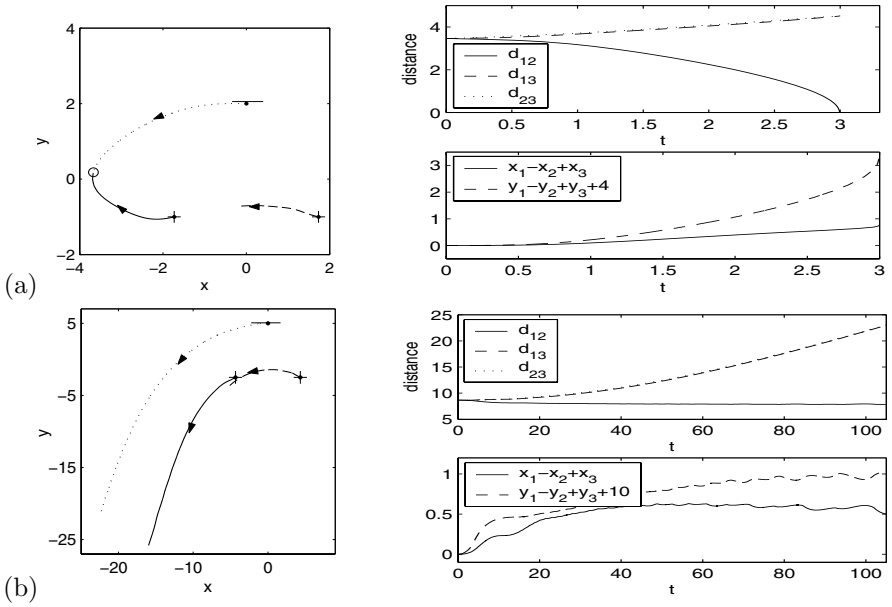

FIG. 23. *Time evolution of vortex centers for the NLSE when the initial condition is chosen as Case* 2 *in Pattern* V *with different a.* (a) $a = 2$. (b) $a = 5$.

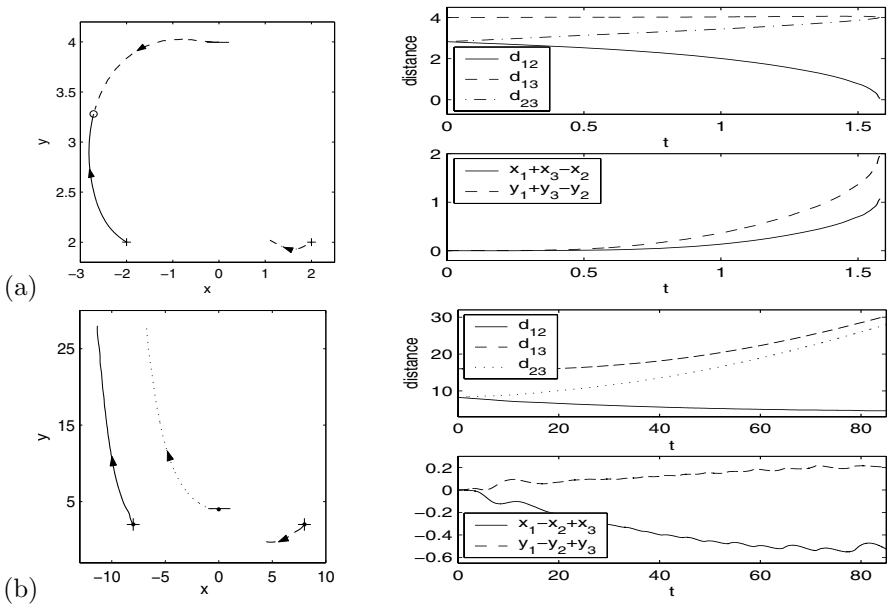

FIG. 24. *Time evolution of vortex centers for the NLSE when the initial condition is chosen as Case* 3 *in Pattern* V *with different a and b.* (a) $a = 2$, $b = 4$. (b) $a = 8$, $b = 4$.

ics law (1.11)–(1.12) is still a reasonable approximation to the vortex motion of the original NLSE in a nonsymmetric initial setup when the N vortices are well separated.

5. Vortex dynamics in the CGLE or in the GLSE with an external potential. In many applications of the GLSE, the physical situation is often more

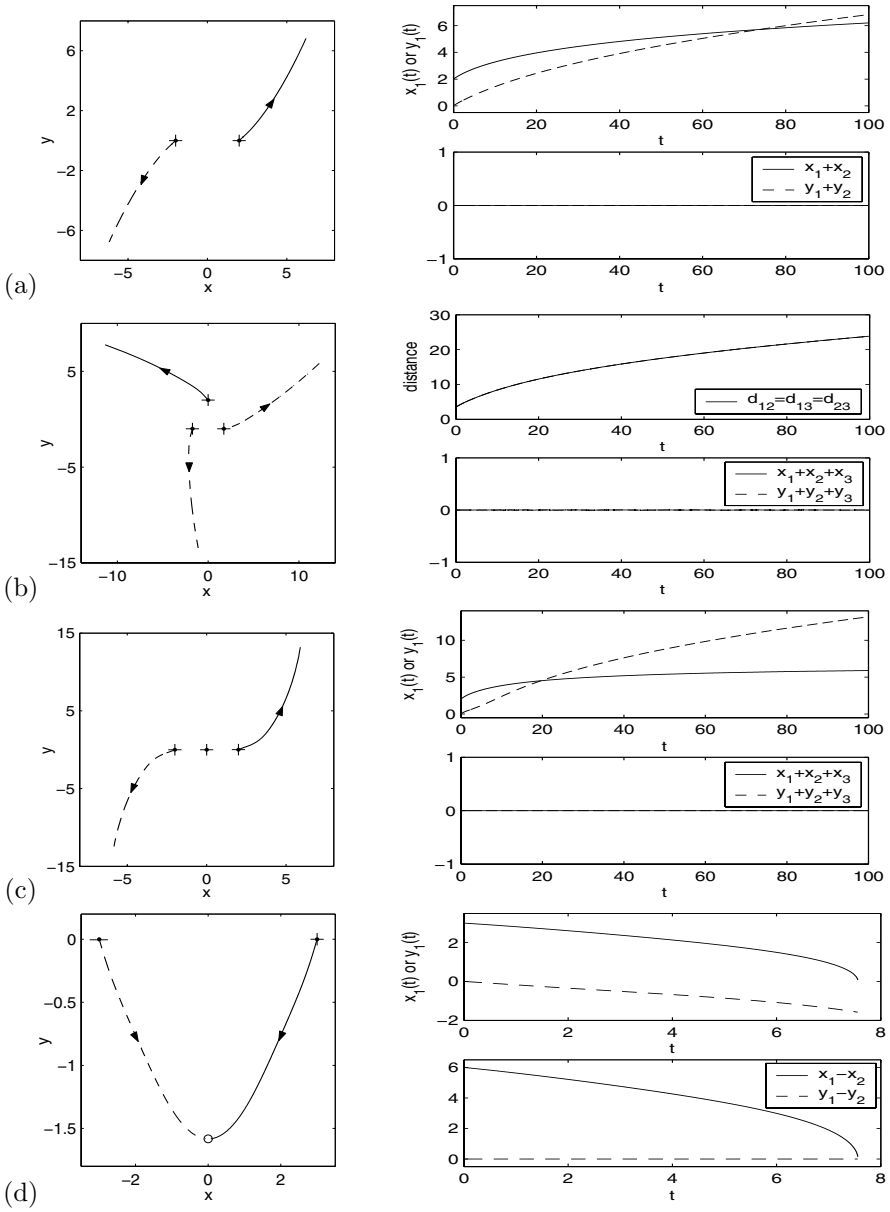

FIG. 25. *Time evolution of vortex centers for the CGLE when the initial condition is chosen as Patterns* I–IV *with different a.* (a) *Pattern* I *with* $N = 2$ *and* $a = 2$. (b) *Pattern* I *with* $N = 3$ *and* $a = 1.5$. (c) *Pattern* II *with* $N = 3$ *and* $a = 2$. (d) *Pattern* IV *with* $a = 3$.

complicated than the GLE and NLSE cases considered in the earlier sections. As an illustration, in this section we report numerical results of vortex interaction in the CGLE and vortex motion in the GLSE with an inhomogeneous external potential.

5.1. Numerical results for vortex dynamics in the CGLE. We take $\alpha = \beta = 1$, $\varepsilon = 1$, and $V(\mathbf{x}) \equiv 1$ in (1.1). Figure 25 shows the various time evolutions of the vortex centers when the initial data in (1.7) are chosen as Patterns I, II, and IV.

Based on Figure 25 and our additional numerical experiments, we can draw the following conclusions for vortex dynamics in the CGLE:

(i) Vortices with the same index undergo repulsive interactions and never collide. The trajectories are combinations of those from the GLE and the NLSE (cf. Figure 25(a), (b), and (c)).

(ii) Two vortices with opposite indices collide after some time t_c (cf. Figure 25(d)) and the collision position is $(0, -d_2)$. The collision time and position depend on the initial distance between the two vortices $d_0 = 2a$. Our numerical results suggest the following relation between them:

$$t_c \approx \frac{1}{8.9837}\, d_0^{2.0655}, \qquad d_1 \approx \frac{1}{4.7781}\, d_0^{1.0184}, \quad \text{with} \quad d_1 = \sqrt{d_0^2 + d_2^2}.$$

In addition, based on the numerical results in Figure 25 it is reasonable to make the following conjecture about the reduced dynamic laws for the interaction of N well-separated vortices with winding number $m_j = +1$ or -1:

$$\mathbf{v}_j(t) := \frac{d\mathbf{x}_j(t)}{dt} = 2 \sum_{l=1,\, l\neq j}^{N} m_l \frac{\mathbf{Q}_j\,(\mathbf{x}_j(t) - \mathbf{x}_l(t))}{|\mathbf{x}_j(t) - \mathbf{x}_l(t)|^2}, \qquad t \geq 0, \tag{5.1}$$

$$\mathbf{x}_j(0) = \mathbf{x}_j^0, \qquad 1 \leq j \leq N, \tag{5.2}$$

where $\mathbf{Q}_j$ is given as

$$\mathbf{Q}_j = \begin{pmatrix} m_j\,\kappa_1 & -\kappa_2 \\ \kappa_2 & m_j\,\kappa_1 \end{pmatrix} = m_j \kappa_1\, I + \kappa_2\, J, \qquad j = 1, 2, \ldots, N,$$

with κ_1 and κ_2 being constants determined from α, β in (1.1) and the initial setup (1.7). Formal derivation of the above reduced dynamics laws (5.1) for the CGLE can be followed from those in [27] for the GLE and NLSE. Again, the nonlinear ODEs (5.1) can be solved analytically as those in section 2.3 for the GLE and section 2.4 for the NLSE when the initial conditions in (5.2) are given by Patterns I–IV in section 2.2. The details are omitted here. For comparison, Figure 26 shows numerical solutions of (5.1) for different initial setups. This figure clearly confirms our conjecture (5.1) about the reduced dynamic laws of the CGLE for the interaction of N well-separated vortices with winding number $m_j = +1$ or -1.

5.2. Vortex motion under an inhomogeneous external potential. The particular external potential we take is of the form

$$V(\mathbf{x}) = \frac{\frac{1}{2} + \gamma_x x^2 + \gamma_y y^2}{1 + \gamma_x x^2 + \gamma_y y^2} = 1 - \frac{1}{2\,(1 + \gamma_x x^2 + \gamma_y y^2)}, \qquad \mathbf{x} \in \mathbb{R}^2, \tag{5.3}$$

where γ_x and γ_y are two positive constants. It is easy to see that $V(\mathbf{x})$ attains its minimum value $1/2$ at the origin $(0, 0)$. Here we study numerically the dynamics of a vortex in the following two cases:

Case I. Isotropic external potential, e.g., $\gamma_x = \gamma_y = 1$ in (5.3).

Case II. Anisotropic external potential, e.g., $\gamma_x = 1$ and $\gamma_y = 5$ in (5.3).

For the GLE, i.e., $\alpha = 1$ and $\beta = 0$ in (1.1), the velocity of the induced motion due to the inhomogeneous impurities was obtained in [17]:

$$\mathbf{v}(t) := \frac{d\mathbf{x}(t)}{dt} = -\nabla \ln V(\mathbf{x}(t)), \quad t \geq 0, \qquad \text{with} \quad \mathbf{x}(0) = \mathbf{x}^0. \tag{5.4}$$

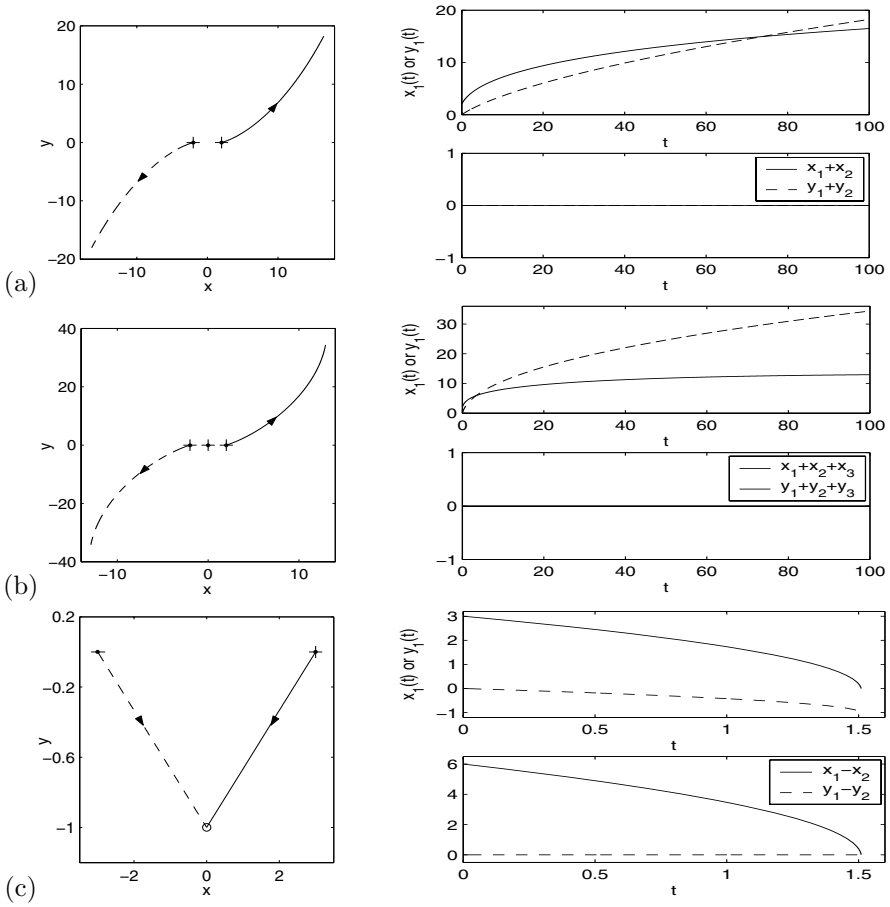

FIG. 26. *Numerical solutions of the reduced dynamical laws* (5.1) *for the CGLE with* $\kappa_1 = 3$ *and* $\kappa_2 = 1$ *for different initial setups.* (a) *Pattern* I *with* $N = 2$ *and* $a = 2$. (b) *Pattern* II *with* $N = 3$ *and* $a = 2$. (c) *Pattern* IV *with* $a = 3$.

This implies that here, the vortex would move to the minimizer of the external potential $V(\mathbf{x})$. Furthermore, if the external potential is isotropic, the trajectory is a segment connecting $\mathbf{x}^0$ and the minimization point of $V(\mathbf{x})$, while for the NLSE and CGLE, the dynamic laws with impurities remain to be established.

The initial condition in (1.2) is chosen as $\psi(\mathbf{x}, 0) = \phi_1\left(\mathbf{x} - \mathbf{x}^0\right)$ for $\mathbf{x} \in \mathbb{R}^2$, where $\phi_1 = \phi_1(\mathbf{x})$ is the vortex state solution (1.4) with winding number $m = +1$ and $\mathbf{x}^0$ is a given point. Figure 27 displays the time evolution of the vortex center in the GLE with $\mathbf{x}^0 = (1, 2)^T$ for different ε, and Figures 28 and 29 show similar results for the CGLE and NLSE, respectively.

From Figures 27–29, we can draw the following conclusions. First, for the GLE and CGLE, the vortex center moves monotonically to the position where the external potential $V(\mathbf{x})$ attains its minimum value (cf. Figures 27 and 28). The speed of the motion depends on the values of the parameter ε. The trajectory of the vortex center depends on the external potential $V(\mathbf{x})$, which agrees with the analytical results for the GLE in [16, 17, 21]. After the vortex reaches the minimum point of the external potential, it always stays at that point, which illustrates the pinning effect. Second,

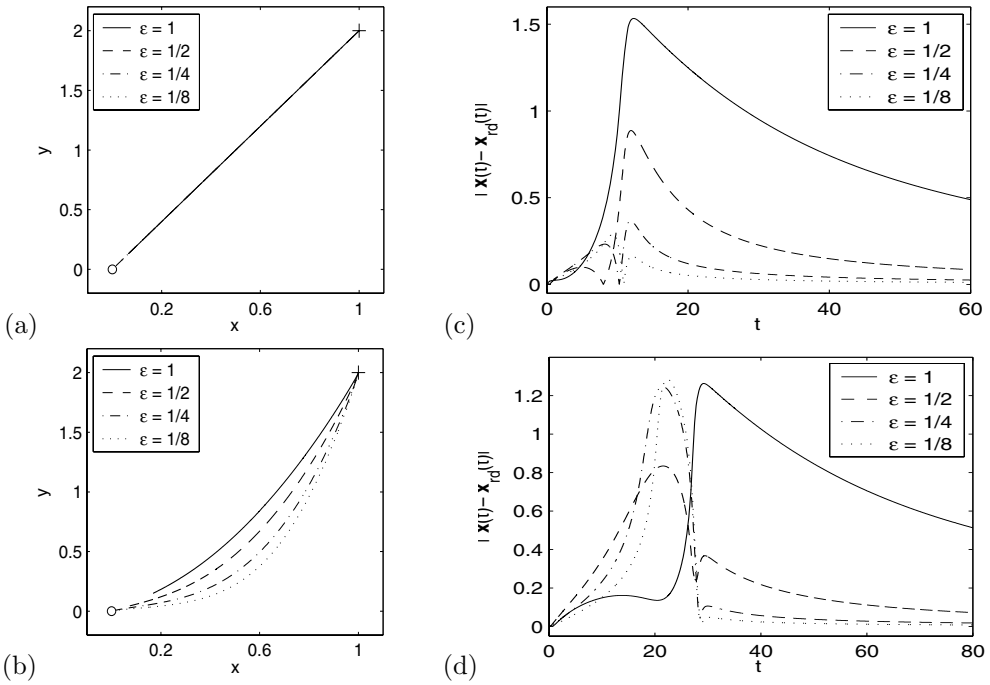

FIG. 27. *Time evolution of the vortex center under an inhomogeneous external driving potential in the GLE.* (a), (b): *Case* I *and* II, *respectively. Trajectory for different* ε. (c), (d): *Errors between the numerical results of the GLE* (*denoted as* $\mathbf{x}(t)$) *and the solution of the reduced dynamic laws* (5.4) (*denoted as* $\mathbf{x}_{\rm rd}(t)$).

for the NLSE, the vortex center moves rotationally clockwise when $m = +1$ and counterclockwise when $m = -1$, to the minimum position of the external potential (cf. Figure 29). The smaller ε, the longer the vortex center stays on a circle. Additional experiments were carried out for Case II. Similar motion patterns were observed, so the results are omitted here.

Based on the numerical results in Figures 28–29, it is reasonable to make the following conjectures about the vortex motion in the NLSE and CGLE: For the NLSE under an inhomogeneous potential, the velocity of the induced motion satisfies (cf. the right-hand side of Figure 29)

$$\mathbf{v}(t) := \frac{d\mathbf{x}(t)}{dt} = -m\kappa\, \mathbf{J}\nabla \ln V(\mathbf{x}(t)), \quad t \geq 0, \qquad \text{with} \quad \mathbf{x}(0) = \mathbf{x}^0, \tag{5.5}$$

where m is the winding number of the vortex, κ is a constant, and $\mathbf{J}$ is the symplectic matrix given in (1.13), while for the CGLE, it can be given by (cf. Figure 28(c),(d))

$$\mathbf{v}(t) := \frac{d\mathbf{x}(t)}{dt} = -\mathbf{Q}\nabla \ln V(\mathbf{x}(t)), \quad t \geq 0, \qquad \text{with} \quad \mathbf{x}(0) = \mathbf{x}^0, \tag{5.6}$$

where the matrix $\mathbf{Q} = m\,\kappa\mathbf{J} + \mathbf{I}$ with κ a constant, and $\mathbf{J}$ and $\mathbf{I}$ are the symplectic matrix in (1.13) and identity matrix, respectively. Their rigorous mathematical justification is not yet available.

6. Conclusion. We have studied the dynamics and interaction of quantized vortices in the Ginzburg–Landau–Schrödinger equation (GLSE) for modeling superconductivity and superfluidity both analytically and numerically. Along the analytical

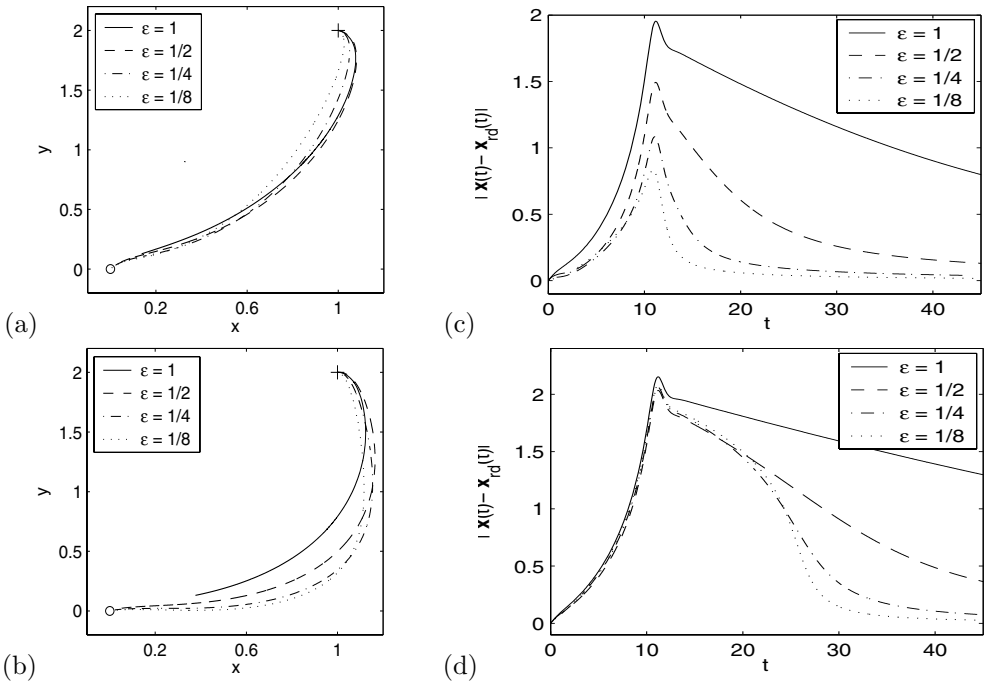

FIG. 28. *Time evolution of the vortex center under an inhomogeneous external driving potential in the CGLE.* (a), (b): *Case* I *and* II*, respectively. Trajectory for different* ε. (c), (d): *Errors between the numerical results of the CGLE* (*denoted as* $\mathbf{x}(t)$) *and the solution of the reduced dynamic laws* (5.6) *with* $\kappa = 1$ (*denoted as* $\mathbf{x}_{\rm rd}(t)$).

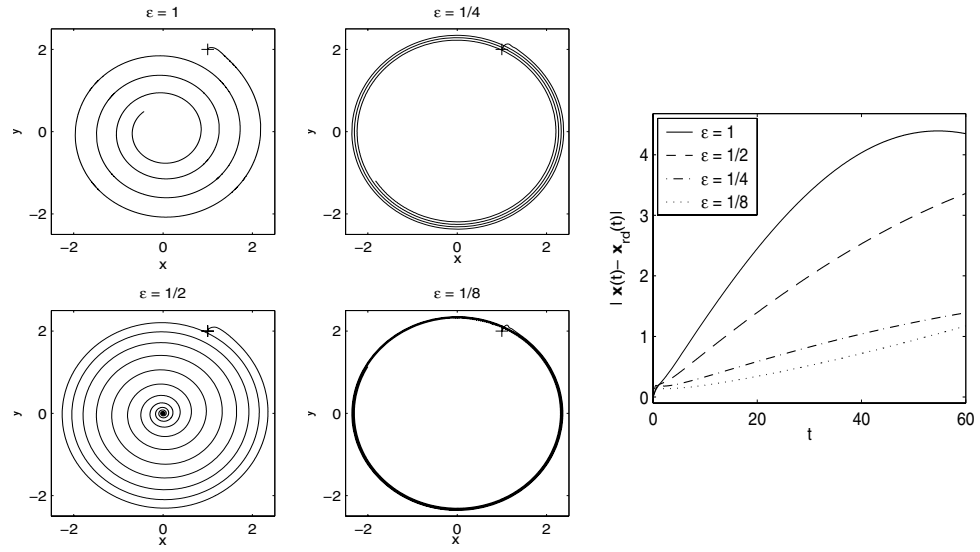

FIG. 29. *Time evolution of the vortex center under an inhomogeneous external driving potential in the NLSE with different* ε *for Case* I. *Left and middle: Trajectory for different* ε. *Right: Errors between the numerical results of the NLSE* (*denoted as* $\mathbf{x}(t)$) *and the solution of the reduced dynamic laws* (5.5) *with* $\kappa = 3$ (*denoted as* $\mathbf{x}_{\rm rd}(t)$).

front, we proved the conservation of the mass center and the signed mass center of N vortex centers governed by the reduced dynamic laws for the Ginzburg–Landau equation (GLE) and nonlinear Schrödinger equation (NLSE), respectively. We also solved analytically the nonlinear ordinary differential equations (ODEs) governing the reduced dynamic laws of the GLE and NLSE for some initial data with symmetrically placed vortices. On the numerical side, by applying an efficient, accurate, and unconditionally stable numerical method for the GLSE with nonzero far-field conditions in two dimensions, we numerically examined issues such as the interaction of vortices and the motion of a vortex under an inhomogeneous external potential in the GLSE. Comparisons between the solutions of the reduced dynamic laws and direct simulation results of the GLSE were provided. Some conclusive findings were obtained, and discussions on numerical and theoretical results were provided for further understanding of vortex interactions in the GLSE. In addition, the vortex motion under an inhomogeneous external potential in the GLSE was investigated numerically for the first time and some conjectures for the motion were made based on our computational findings. In the future, we will extend our efficient and accurate numerical method to the study of the dynamics and the interaction of vortex line states in three dimensions and in bounded domains for the GLSE.

REFERENCES

[1] I. Aranson and L. Kramer, *The world of the complex Ginzburg-Landau equation*, Rev. Modern Phys., 74 (2002), pp. 99–133.

[2] W. Bao, *Numerical methods for the nonlinear Schrödinger equation with nonzero far-field conditions*, Methods Appl. Anal., 11 (2004), pp. 367–387.

[3] W. Bao, Q. Du, and Y. Zhang, *Dynamics of rotating Bose–Einstein condensates and its efficient and accurate numerical computation*, SIAM J. Appl. Math., 66 (2006), pp. 758–786.

[4] W. Bao and Y. Zhang, *Dynamics of the ground state and central vortex states in Bose-Einstein condensation*, Math. Models Methods Appl. Sci., 15 (2005), pp. 1863–1896.

[5] W. Bao and Y. Zhang, *Dynamics of the center of mass in rotating Bose-Einstein condensates*, Appl. Numer. Math., 57 (2007), pp. 697–709.

[6] P. Bauman, C. Chen, D. Phillips, and P. Sternberg, *Vortex annihilation in nonlinear heat flow for Ginzburg-Landau systems*, European J. Appl. Math., 6 (1995), pp. 115–126.

[7] S. J. Chapman and G. Richardson, *Motion of vortices in type* II *superconductors*, SIAM J. Appl. Math., 55 (1995), pp. 1275–1296.

[8] J. E. Colliander and R. L. Jerrard, *Vortex dynamics for the Ginzburg–Landau–Schrödinger equation*, Internat. Math. Res. Notices, 7 (1998), pp. 333–358.

[9] Q. Du, *Finite element methods for the time dependent Ginzburg-Landau model of superconductivity*, Comput. Math. Appl., 27 (1994), pp. 119–133.

[10] Q. Du, *Numerical approximations of the Ginzburg-Landau models for superconductivity*, J. Math. Phys., 46 (2005), 095109.

[11] Q. Du, M. D. Gunzburger, and J. S. Peterson, *Analysis and approximation of the Ginzburg–Landau model of superconductivity*, SIAM Rev., 34 (1992), pp. 54–81.

[12] Q. Du, M. Gunzburger, and J. Peterson, *Computational simulation of type*-II *superconductivity including pinning phenomena*, Phys. Rev. B, 51 (1995), pp. 16194–16203.

[13] Q. Du and W. Zhu, *Stability analysis and application of the exponential time differencing schemes*, J. Comput. Math., 22 (2004), pp. 200–209.

[14] W. E, *Dynamics of vortices in Ginzburg-Landau theories with applications to superconductivity*, Phys. D, 77 (1994), pp. 383–404.

[15] R. Jerrard and H. M. Soner, *Dynamics of Ginzburg-Landau vortices*, Arch. Rational Mech. Anal., 142 (1998), pp. 99–125.

[16] H. Y. Jian, *The dynamical law of Ginzburg-Landau vortices with a pinning effect*, Appl. Math. Lett., 13 (2000), pp. 91–94.

[17] H. Y. Jian and B. H. Song, *Vortex dynamics of Ginzburg-Landau equations in inhomogeneous superconductors*, J. Differential Equations, 170 (2001), pp. 123–141.

[18] O. Lange and B. J. Schroers, *Unstable manifolds and Schrödinger dynamics of Ginzburg-Landau vortices*, Nonlinearity, 15 (2002), pp. 1471–1488.
[19] F.-H. Lin, *Some dynamical properties of Ginzburg-Landau vortices*, Comm. Pure Appl. Math., 49 (1996), pp. 323–359.
[20] F.-H. Lin, *Complex Ginzburg-Landau equations and dynamics of vortices, filaments, and codimension-2 submanifolds*, Comm. Pure Appl. Math., 51 (1998), pp. 385–441.
[21] F.-H. Lin and Q. Du, *Ginzburg–Landau vortices: Dynamics, pinning, and hysteresis*, SIAM J. Math. Anal., 28 (1997), pp. 1265–1293.
[22] F.-H. Lin and J. X. Xin, *On the dynamical law of the Ginzburg-Landau vortices on the plane*, Comm. Pure Appl. Math., 52 (1999), pp. 1189–1212.
[23] F.-H. Lin and J. X. Xin, *On the incompressible fluid limit and the vortex motion law of the nonlinear Schrödinger equation*, Comm. Math. Phys., 200 (1999), pp. 249–274.
[24] F.-H. Lin and J. X. Xin, *A unified approach to vortex motion laws of complex scalar field equations*, Math. Res. Lett., 5 (1998), pp. 455–460.
[25] P. Mironescu, *Les minimiseurs locaux pour l'équation de Ginzburg-Landau sont à symétrie radiale*, C. R. Acad. Sci. Paris Sér. I Math., 323 (1996), pp. 593–598.
[26] P. Mironescu, *On the stability of radial solutions of the Ginzburg-Landau equation*, J. Funct. Anal., 130 (1995), pp. 334–344.
[27] J. C. Neu, *Vortices in complex scalar fields*, Phys. D, 43 (1990), pp. 385–406.
[28] J. C. Neu, *Vortex dynamics of the nonlinear wave equation*, Phys. D, 43 (1990), pp. 407–420.
[29] Y. N. Ovchinnikov and I. M. Sigal, *Ginzburg-Landau equation* I. *Static vortices*, in Partial Differential Equations and Their Applications, CRM Proc. Lecture Notes 12, AMS, Providence, RI, 1997, pp. 199–220.
[30] Y. N. Ovchinnikov and I. M. Sigal, *The Ginzburg-Landau equation* III. *Vortex dynamics*, Nonlinearity, 11 (1998), pp. 1277–1294.
[31] Y. N. Ovchinnikov and I. M. Sigal, *Long-time behavior of Ginzburg-Landau vortices*, Nonlinearity, 11 (1998), pp. 1295–1309.
[32] Y. N. Ovchinnikov and I. M. Sigal, *Asymptotic behavior of solutions of Ginzburg-Landau and related equations*, Rev. Math. Phys., 12 (2000), pp. 287–299.
[33] Y. N. Ovchinnikov and I. M. Sigal, *Symmetry-breaking solutions of the Ginzburg-Landau equation*, J. Exp. Theor. Phys., 99 (2004), pp. 1090–1107.
[34] E. Sandier, *The symmetry of minimizing harmonic maps from a two-dimensional domain to the sphere*, Ann. Inst. H. Poincaré Anal. Non Linéaire, 10 (1993), pp. 549–559.
[35] M. I. Weinstein and J. Xin, *Dynamics stability of vortex solutions of Ginzburg-Landau and nonlinear Schrödinger equations*, Comm. Math. Phys., 180 (1996), pp. 389–428.
[36] Y. Zhang, W. Bao, and Q. Du, *Numerical simulation of vortex dynamics in Ginzburg–Landau–Schrödinger equation*, European J. Appl. Math., to appear.